Climate Dynamics (2001) 18: 103–122

R. Colman · J. Fraser · L. Rotstayn

Climate feedbacks in a general circulation model incorporating prognostic clouds

Received: 15 June 2000 / Accepted: 10 January 2001

Abstract This study performs a comprehensive feedback analysis on the Bureau of Meteorology Research Centre General Circulation Model, quantifying all important feedbacks operating under an increase in atmospheric CO_2. The individual feedbacks are analysed in detail, using an offline radiation perturbation method, looking at long- and shortwave components, latitudinal distributions, cloud impacts, non-linearities under $2xCO_2$ and $4xCO_2$ warmings and at interannual variability. The water vapour feedback is divided into terms due to moisture height and amount changes. The net cloud feedback is separated into terms due to cloud amount, height, water content, water phase, physical thickness and convective cloud fraction. Globally the most important feedbacks were found to be (from strongest positive to strongest negative) those due to water vapour, clouds, surface albedo, lapse rate and surface temperature. For the longwave (LW) response the most important term of the cloud 'optical property' feedbacks is due to the water content. In the shortwave (SW), both water content and water phase changes are important. Cloud amount and height terms are also important for both LW and SW. Feedbacks due to physical cloud thickness and convective cloud fraction are found to be relatively small. All cloud component feedbacks (other than height) produce conflicting LW/SW feedbacks in the model. Furthermore, the optical property and cloud fraction feedbacks are also of opposite sign. The result is that the net cloud feedback is the (relatively small) product of conflicting physical processes. Non-linearities in the feedbacks are found to be relatively small for all but the surface albedo response and some cloud component contributions. The cloud impact on non-cloud feedbacks is also discussed: greatest impact is on the surface albedo, but impact on water vapour feedback is also significant. The analysis method here proves to be a powerful tool for detailing the contributions from different model processes (and particularly those of the clouds) to the final climate model sensitivity.

R. Colman (✉) · J. Fraser
Bureau of Meteorology Research Centre,
GPO Box 1289 K Melbourne Victoria,
3001, Australia
E-mail: rzc@bom.gov.au

L. Rotstayn
CSIRO Atmospheric Research, Private Bag No 1,
Aspendale, 3195, Australia

Current affiliation: J. Fraser
National Meteorological and Oceanographic Centre,
Bureau of Meteorology, Melbourne, 3000, Australia

1 Introduction

There remains a good deal of uncertainty as to the magnitude of the climate change expected due to anthropogenic greenhouse gas emissions (IPCC 1996). To a large degree this uncertainty is in turn due to uncertainties in the nature and the strength of key climate feedbacks, as simulated by general circulation models (GCMs). The quantification and understanding of these feedbacks, therefore, remain principal goals of climate change research.

The magnitude of GCM feedbacks has been inferred using a number of different diagnostic techniques. These range from the use of simplified (1D or 2D) models, either alone (e.g. Somerville and Remer 1984) or forced by time and global mean GCM output (e.g. Hansen et al. 1984; Gong et al. 1994), through to the performance of multiple GCM experiments designed to isolate particular feedbacks (e.g. Taylor and Ghan 1992; Mitchell et al. 1989). The climate forcing used has ranged from idealised fixed sea surface forcing (e.g. Cess et al. 1990, 1996) through to full solar and greenhouse gas experiments (e.g. Roeckner et al. 1987; Le Treut et al. 1994).

A clear aim of such feedback analysis is to understand GCM climate 'sensitivity' (defined as the equilibrium response to a doubling of atmospheric CO_2, IPCC 1990). Many analysis methods however, are limited in their usefulness for quantifying GCM feedbacks appropriate for CO_2 forcing. For example, the temporal

and spatial averaging required for simplified models may perhaps be suitable for evaluating some feedbacks (e.g. total water vapour or temperature) but is problematic for others (e.g. clouds or surface albedo). For cloud amounts in particular, Wetherald and Manabe (1988) found that the use of time averages distorted analysed feedbacks because of non-linearities inherent in cloud/radiation interactions, even in a full GCM. Taylor and Ghan (1992) noted that temporal and spatial averaging of such parameters as cloud liquid water was unsafe. These findings throw into doubt many of the conclusions drawn on cloud feedbacks using simplified models or, for example, even by GCM experiments which hold cloud water fixed using zonal or temporal means.

The type of climate forcing used is also very important. For example, although extremely useful for comparisons between models (e.g. Cess et al. 1990) or for multiple experiments with the same model (e.g. Colman and McAvaney 1997; Rotstayn 1999) it is known that climate feedbacks inferred from idealised experiments may not relate closely to feedbacks occurring under more 'realistic' greenhouse gas forcing (Senior and Mitchell 1993).

The number of estimates of model feedbacks, then, using both realistic forcing scenarios and robust diagnostic methods is relatively small. Furthermore, due to temporal and/or spatial averaging, accurate estimates of components contributing to the final cloud feedback are also scarce. Two principal aims of this study are: to provide a feedback analysis method suitable for the diagnosis of all important feedbacks, including those of the cloud sub-components, and then to comprehensively identify and evaluate the feedbacks in one GCM under CO_2 forcing.

The closest consensus on model feedbacks exists for the net 'clear sky' feedback, diagnosed under idealised forcing (Cess et al. 1990, 1996). The clear sky response approximates the sum of the surface temperature, lapse rate and water vapour feedbacks, but is dominated overall by the surface temperature (i.e. Planck function) term. Albedo feedback is suppressed. The applicability of the result to doubled CO_2 forcing is also open to some doubt, due to the idealised nature of the forcing.

The individual clear sky terms have been only relatively rarely evaluated for CO_2 (or solar) climate forcing in GCMs. The water vapour (or water vapour combined with lapse rate) feedback was found to be the strongest positive feedback under CO_2 forcing in GCM studies by Wetherald and Manabe (1988) and Le Treut et al. (1994). Two radiative convective model (RCM) studies (Hansen et al. 1984; Gong et al. 1994) further subdivided the water vapour response into terms due to total column water vapour, and to the height distribution, finding the former dominated the latter by around 2 to 1 (although the use of area and time mean clouds and water vapour increase the uncertainty of these findings). The lapse rate feedback has been evaluated less frequently, but has been found to be negative in most models, due to the decrease in the saturated adiabatic lapse rate with increasing temperature (Arking 1991). Large uncertainties remain in its overall magnitude, as the feedback changes sign between low and high latitudes, so the net result is the (smaller) sum of competing effects. Uniform sea surface temperature (SST) perturbation experiments appear to substantially distort the lapse rate feedback (Colman and McAvaney 1997).

The surface albedo feedback is suppressed in fixed season experiments so it is not included in the clear sky feedback of Cess et al. (1990). It has been evaluated for CO_2 experiments using a number of models (e.g. Ingram et al. 1989), and has been found to be positive (as expected) and generally much weaker than the water vapour feedback. Ingram et al. (1989) point out that care must be taken on the method used for evaluating albedo feedback when area and time averages are taken, indicating that RCM estimates in particular may be misleading.

Cloud feedbacks remain the most difficult to evaluate, due both to the complexity of the cloud responses involved, and the analysis difficulty arising from non-linearities in the cloud/radiative response (Wetherald and Manabe 1988; Gong et al. 1994). This is particularly unfortunate, as cloud feedback differences are thought to be responsible for much of the spread in climate sensitivity (Cess et al. 1990) and hence a clear understanding of the processes contributing to the final cloud feedback is very important. Under climate perturbations we may anticipate changes in cloud amount, vertical distribution, depth and type (e.g. convective or stratiform). Changes may also occur to the cloud optical properties from changes in total (and relative) water and ice contents and the size or number of cloud particles. Perhaps unsurprisingly, estimates of the total cloud feedback even under idealised climate forcing show a very wide range over different GCMs. That range appears to have decreased in recent years (Cess et al. 1996), although this apparent improvement still encompasses very large differences in the estimated shortwave (SW) and longwave (LW) components.

Feedback estimates of some cloud processes have been performed, and help to identify some common features (even if not agreeing on their magnitudes). Global cloud fraction tends to decrease under doubled CO_2 forcing, leading to partially compensating SW and LW feedbacks. The LW response, however, is also sensitive to an overall increase in the height of the highest cloud, contributing an offsetting positive LW feedback. Most separate estimates of cloud amount and height feedback have so far only been made using either RCMs (Hansen et al. 1984; Gong et al. 1994) or simplified climate forcing (Colman et al. 1997), and only one CO_2 study with a 3D GCM feedback analysis has been attempted (Wetherald and Manabe 1988). The separation is important, however, as both RCM and GCM studies suggest that the height change feedback may be an important (or even the dominant) component in the net cloud fraction feedback. Note that of course the RCM evaluation of cloud amount and height feedbacks (cal-

culated using adjusted global or zonal mean cloud fraction changes at each level) is open to substantial doubt because of the averaging involved (Wetherald and Manabe 1988).

Inclusion of cloud liquid and ice water changes further complicates cloud feedback and the diagnosis of it. There is an expectation that the cloud liquid and ice water will increase overall in a warmer climate (Platt 1989; Betts and Harshvardhan 1987), although Tseliodis et al. (1998) note evidence for decreases in the liquid water content of low clouds in low latitudes in both observations and models.

Where water content increases occur, accompanying increases in cloud albedo and emissivity have been found to lead to offsetting negative (SW) and positive (LW) feedbacks (Somerville and Remer 1984; Schlesinger and Roeckner 1988). Different studies, however, disagree over the competing strengths of these two processes, as well as their strengths relative to the cloud fraction feedback (Lee et al. 1997; Senior and Mitchell 1993; Roeckner et al. 1987). Further uncertainties result from the difficulty in diagnosing optical properties from time or area mean cloud liquid water (Taylor and Ghan 1992). This throws into question analysis done with simple models (e.g. Somerville and Remer 1984) or even with GCMs using fixed optical properties determined from zonal and temporal mean cloud liquid water (e.g. Taylor and Ghan 1992).

Equally as important as cloud water contents for total cloud feedback may be changes in the phase of the cloud water substance. In a warmer climate cloud ice amounts may be expected to decrease relative to liquid water. In one GCM study, Li and Le Treut (1992) found this cloud water phase change to have a major impact on their total cloud feedback. Other cloud feedbacks, such as those due to cloud type changes, appear to not yet have been addressed in GCM studies.

The overall aim of the present study, then, is twofold. Firstly it seeks to extend feedback diagnostic methods to include those processes which contribute to total cloud feedback. Secondly it aims to produce a comprehensive feedback analysis for one GCM, using a state of the art prognostic cloud scheme with physically based optical properties, under CO_2 forcing. This includes 'standard' feedbacks, such as temperature, lapse rate, water vapour and surface albedo, but the emphasis will be on a detailed cloud feedback diagnosis covering amounts, height, water content, ice fraction, temperature (i.e. physical cloud thickness) and convective cloud fraction. The reason for this emphasis is that a clear separation of the net cloud feedback into these components has not previously been carried out on GCM results. Both $2xCO_2$ and $4xCO_2$ forcing will be considered, to examine the robustness of the model feedbacks under a broad range of climate warming scenarios.

Of course, the strength of each feedback, particularly those related to clouds may be expected to vary between models, and may be dependent on details of the cloud scheme (Mitchell et al. 1989). It is notable, however, that using the present cloud parametrisation, Rotstayn (1999) found cloud feedbacks to be surprisingly insensitive to relatively broad variations in most parameter settings. Yao and Del Genio (1999) also found total cloud feedback to be relatively insensitive to cloud parametrisation changes, although this was the net result of large but offsetting LW and SW impacts. If such findings were common to many other models, then this would have implications for the origin of inter model cloud feedback differences. Thus it may suggest that changes other than to cloud parametrisations may be a significant source of differences in cloud feedbacks and associated climate sensitivity (a point made by Colman and McAvaney 1997). Although not directly addressing this latter point, it is hoped that the present analysis may serve to illuminate the relative importance in a range of different processes in determining final climate sensitivity, which should be applicable to other models, and may serve as a benchmark for similar future studies.

Section 2 will describe the climate change experiments that were performed and the analysis procedure used to determine the feedbacks. Section 3 will present the results of the feedback analysis, and Sect. 4 will present some concluding discussion.

2 Model and feedback analysis method

2.1 Model and experiment

The model is a version of the BMRC "unified" model run at a horizontal resolution of rhomboidal wave 21, with 17 vertical levels. The present version of the model has surface boundary layer parameterisations based on the formulations of Louis (1983). Oceanic evaporation is enhanced over low wind regions according to the formulation of Miller et al. (1992). Vertical diffusion also follows the stability dependent form of Louis (1983) as modified by McAvaney and Hess (1996). Gravity wave drag is determined using the formulation of Palmer et al. (1986). The LW radiation scheme used is a modified version of the Fels-Schwarzkopf scheme developed at the Geophysical Fluid Dynamics Laboratory (GFDL) (Schwarzkopf and Fels 1991). Shallow convection is modelled by an enhancement to vertical diffusion following Tiedtke (1988). Penetrative convection is parameterised using the mass flux scheme of Tiedtke (1989). Soil moisture is represented by single layer "bucket" model with a field capacity of 150 mm after Manabe and Holloway (1975).

The GCM was coupled with a "Q-flux" corrected 50 m deep mixed layer ocean and a thermodynamic sea-ice model. Three experiments were performed, with atmospheric CO_2 levels specified at 330, 660 and 1320 parts per million, with the model then run to equilibrium. Annual mean warmings in the 2x and $4xCO_2$ experiments (averaged over 15 years) were 2.74 °C and 5.58 °C respectively relative to the $1xCO_2$.

The model includes the Rotstayn (1997) prognostic cloud scheme for stratiform clouds. Given the emphasis on cloud feedbacks and on cloud impacts on non-cloud feedbacks, the cloud scheme will be described in a little more detail. Features of the scheme include two prognostic variables (cloud liquid water and ice) with physically based treatment of associated cloud microphysical processes. A triangular probability function is assumed for the subgrid scale distribution of moisture within a gridbox. Cloud formation is based on the statistical condensation scheme of Smith (1990). Clouds are permitted at all model levels, except the lowest.

An additional diagnostic treatment of convective clouds is included, with the fraction of cloud based on the convective rainfall rate. There is currently only vertical advection of cloud water variables by the model dynamics.

The SW cloud optical properties are calculated as a function of visible optical depth τ_v, and effective radius r_e using a 4-band delta-Eddington scheme for water clouds (Slingo 1989) with a similar scheme for ice clouds. For water clouds

$$\tau_v = \frac{3}{2} \cdot \frac{LWC}{\rho_l r_e} \cdot \mathrm{d}z \tag{1}$$

where LWC is the cloud liquid water content, dz is the thickness of the cloud, ρ_l is the density of water and r_e is the effective radius of the cloud drops.

The effective radius, based on the formulation of Martin et al. (1994), is given by

$$r_e = \left(\frac{3}{2} \cdot \frac{LWC}{\rho_l \pi k C_{\mathrm{drop}}} \cdot \mathrm{d}z \right)^{1/3} \tag{2}$$

where C_{drop} is a prescribed drop concentration, (100 cm^{-3} for maritime clouds and 500 cm^{-3} for continental clouds) and k is a constant relating effective radius with droplet mean volume radius ($k = 0.8$ over ocean, 0.67 over land). Liquid water content is given by

$$LWC = \frac{\rho_a \cdot w_l}{C(1 - f_i)} \tag{3}$$

where ρ_a is the air density, w_l the cloud liquid water mixing ratio, C the total cloud fraction, and f_i the fraction of cloud comprised of ice in the grid box. The calculation of f_i is driven primarily by the relative difference between the saturation vapour pressures with respect to ice and liquid water. Since this quantity is a strong function of temperature, f_i tends to increase with decreasing temperature (Rotstayn 1997).

For ice clouds (following Platt 1994) the optical depth is specified by:

$$\tau_v = 0.032(IWC)^{1/3} \cdot \mathrm{d}z \tag{4}$$

where

$$IWC = \frac{\rho_a w_i}{C f_i} \tag{5}$$

where w_i is the cloud ice water mixing ratio. Consistent with Eq. (1), the effective radius is in turn given by

$$r_e = \frac{3}{2} \cdot \frac{IWC}{\rho_i \tau_v} \cdot \mathrm{d}z \tag{6}$$

where ρ_i is the density of ice.

In the longwave (LW) the cloud emissivity, ε, is specified by

$$\varepsilon = 1 - \mathrm{e}^{-K\tau_a} \tag{7}$$

where K is the optical depth diffusivity factor (derived from Platt and Stephens 1980) and τ_a the infrared optical depth, in turn given by

$$\tau_a = \kappa \tau_v \tag{8}$$

where $\kappa = 0.4$ and 0.5 for water and ice clouds respectively.

Combining Eqs. (1) to (3), it is clear that both SW and LW optical depths increase with increases in w_l and w_i, the liquid and ice water mixing ratios (for given fractions of liquid and ice cloud). For increases in temperature, but with fixed values of w_l and w_i, competing effects occur on optical depth. The absolute cloud depth, dz, increases with temperature, while liquid and ice water contents decrease, due to their dependence on air density. This compensation is exact as formulated for liquid clouds, but for ice clouds the net effect is that optical depth increases with temperature to the two thirds power. In the case of water clouds the effective radius, r_e, is insensitive to temperature.

Finally, in the SW, the cloud albedo is a function of both liquid water content and r_e as well as the fraction of cloud diagnosed as convective. For the convective fraction of cloud, cloud albedo is reduced by approximately 20% below that value calculated for large scale cloud (see Rotstayn 1997).

2.2 Feedback analysis

The feedback method here is an extension of that described in Colman et al. (1997), with the discussion of individual field substitutions confined to those that are handled differently.

We assume that the top of atmosphere (TOA) radiation, R, at a given location in the model can be written (where the tilde '$\sim$' denotes the vertical profile of a variable):

$$R = R(\tilde{T}, \tilde{q}, \tilde{C}, \alpha, \tilde{CO}_2, \tilde{O}_3) \tag{9}$$

where $\tilde{T}$ is the atmospheric temperature profile (including the surface), $\tilde{q}$ is the specific humidity profile, $\tilde{C}$ is the vertical cloud distribution including optical properties, α is the surface albedo and $\tilde{CO}_2$ and $\tilde{O}_3$ represent the carbon dioxide and ozone amounts respectively. The "feedbacks" in the model are those processes that alter $\tilde{T}, \tilde{q}, \tilde{C}$ or α as a function of, say, the surface temperature, T_* and thus which also alter R as a function of T_* (see Colman et al. 1997) after some climate perturbation (say a change in CO_2).

We assume, for a small climate perturbation, we can write:

$$\delta R \approx \delta R_{\tilde{T}} + \delta R_{\tilde{q}} + \delta R_{\tilde{C}} + \delta R_{\alpha} + \delta R_{\tilde{CO}_2} \tag{10}$$

where δR_{x} is the radiation change due to the perturbation to field x.

The method of calculation was similar to that of Colman et al. (1997), with radiative perturbations determined by off line radiation calculation, substituting one field at a time from the perturbed into the control climate. The radiation is then differenced from the unperturbed case, and a global or zonal average taken.

A further set of substitutions was made in all cases, in which the perturbed and control climates were interchanged and the radiation perturbations re-calculated. Half the difference of the radiation impact from the two mirror substitutions is a more useful measure of the impact of the field change than a single substitution, because the radiation pertubation due to the induced field decorrelation is thereby largely subtracted off. Colman and McAvaney (1997) contains a full discussion of this point. In the present study the perturbations to $\tilde{T}$ and $\tilde{q}$ fields were conceptually simplified into a "mean" horizontal change, and a net "vertical" perturbation, so we assume:

$$\begin{aligned} \delta R_{\tilde{T}} &\approx \delta R_{T_*} + \delta R_{\tilde{\Gamma}} \\ \delta R_{\tilde{q}} &\approx \delta R_{qA} + \delta R_{\tilde{q}H} \end{aligned} \tag{11}$$

where T_* is the surface temperature, Γ the vertical temperature profile ("lapse rate"), q_A the total column water vapour and q_H the water vapour "lapse rate" (see Hansen et al. 1984; Gong et al. 1994; Schlesinger 1988 for similar definitions). The perturbation to $\tilde{q}$ to calculate water vapour amount feedback consists of a uniform percentage change in specific humidity at all levels (corresponding to the percentage change in total precipitable water). Note also that the change in temperature lapse rate is confined to the troposphere, to ensure that there is an (approximately) equilibrated stratosphere in line with the convention of including stratospheric temperature changes in the CO_2 "forcing" term rather than attributing them to lapse rate changes (Hansen et al. 1981). The method of water vapour feedback division into q_A and q_H is identical to that in Colman et al. (1997).

2.3 Cloud feedback

The radiative response of the model to changes in clouds is much more complex than that of the other processes already discussed, so the feedback calculation method will be described in some detail. We assume we can write

$$\delta R_{\tilde{C}} \approx \delta R_{\tilde{C}_F} + \delta R_{\tilde{C}_O} \tag{12}$$

where C_O represents the change in optical properties and C_F the cloud fraction changes. The first calculation, to determine total

cloud feedback ($\delta R_{\tilde{C}}$), substituted all cloud properties: cloud fraction at each model level, liquid and ice water mixing ratios, convective cloud fraction and cloud temperature. The second calculation, to isolate the impact of the cloud fraction changes alone ($\delta R_{\tilde{C}_F}$) replaced cloud amounts at each level in the control climate with those from the perturbed. In-cloud liquid and ice water mixing ratios were retained from the control by scaling grid box mean values by the reciprocal of the cloud fraction change. Thus at each model level,

$$w_l \rightarrow Z w_l \tag{13}$$

where

$$Z = C'/C$$

where C is the cloud fraction, w_l is the grid box mean cloud liquid water mixing ratio and the prime denotes the perturbed climate. The ice and convective cloud mixing ratio fields (w_i, w_c) were handled similarly.

The only complication to this substitution occurred if the cloud fraction in the control climate was zero, yet non-zero in the perturbed. In this case w_l, w_i and w_c were taken from the perturbed climate. To clearly separate the cloud fraction term from the total cloud feedback, it is clear that this latter occurrence needs to be minimised. Indeed, for upper level clouds it can occur reasonably frequently, as cloud may be present only over a relatively small fraction of the globe at a given instant (e.g. around 10% for clouds at sigma level 0.188), although this is somewhat offset by a tendency for the regions of preferred cloud development in both climates (e.g. the Inter Tropical Convergence Zone) to be roughly coincident.

To evaluate the right hand side of Eq. (12) as often as possible, the substitution algorithm was extended to search for cloud from immediately surrounding grid points, then from earlier similar-time archives (0, ± 3 hours) taken from the same calendar month. This ensures 'corresponding' cloud is found close to 100% of the time at all model levels. The final feedback values obtained were not found to be sensitive to the precise details (e.g. the order) of the search algorithm.

To calculate $\delta R_{\tilde{C}_O}$ directly, cloud fractions were retained from the control and the fields w_l, w_i and w_c were modified as follows:

$$w_x \rightarrow \frac{1}{Z} w'_x \tag{14}$$

where x is l, i or c. By this method, the cloud amounts are retained from the control, but the in-cloud liquid and ice water mixing ratios and the relative fraction of convective cloud become that of the perturbed climate.

For the cloud fraction changes we note that a common feature of many climate change experiments (including the present ones) is the increase in cloud fractions at some (often high) levels, and decrease at others (often low) resulting in an effective change in mean cloud height. Here we conceptually divide this (potentially complex) change into two terms: one due to change in total cloud amount (C_A) (as seen at the TOA) and the second due to the change in the vertical distribution of the clouds, taken as the cloud height, C_H.

In the present case the C_A perturbation was performed by scaling cloud at each level in the "control" by a factor, (f), such that the total cloud (t) becomes that of the perturbed climate (t'). Note that due to the random overlap assumption of the clouds between levels, in general $f \neq t'/t$. In the present calculations, f was calculated directly at each point by an iterative technique. The cloud height feedback was then determined as a residual (i.e. $C_F - C_A$).

Clouds at any particular model layer are assumed to fill that layer. Since the levels are not evenly distributed in the vertical there will be a different cloud "depth" (and therefore optical depth) for a given cloud fraction at different heights. This cloud depth term is implicitly included in our C_H variable due to the present means of its calculation.

To explore the causes of the changes arising from optical property perturbations in more detail we assume we can write

$$\delta R_{\tilde{C}_O} \approx \delta R_{\tilde{C}_W} + \delta R_{\tilde{C}_P} + \delta R_{\tilde{C}_C} + \delta R_{\tilde{C}_T} \tag{15}$$

where $\tilde{C}_W$ is the total water (liquid plus ice) content of the clouds, $\tilde{C}_P$ represents a phase breakdown of the total cloud water between water and ice (i.e. $w_l/(w_l + w_i)$), $\tilde{C}_C$ is the fraction of convective clouds, and $\tilde{C}_T$ is the in-cloud temperature.

To calculate $\delta R_{\tilde{C}_W}$ the fields w_l, w_i and w_c were scaled in the control by a factor r/Z, where

$$r = \frac{w'_l + w'_i}{w_l + w_i} \ . \tag{16}$$

By this method the relative fractions of w_l and w_i and the relative fraction of convective cloud are retained from the control climate, but the total in-cloud water substance becomes that of the perturbed climate. If cloud fraction is zero in the perturbed climate ($w'_l + w'_i = 0$), then r/Z is set to 1 (i.e. the water content is unchanged).

To calculate $\delta R_{\tilde{C}_P}$ the mixing ratios of liquid and ice water were modified such that

$$\begin{aligned} w_l &\rightarrow \frac{1}{r} w'_l \\ w_i &\rightarrow \frac{1}{r} w'_i \ . \end{aligned} \tag{17}$$

Thus the total water substance in the clouds was unmodified, but the fraction which is frozen reflects that of the perturbed climate rather than the control.

To calculate $\delta R_{\tilde{C}_C}$, w_c is scaled by a factor $(w'_c/w_c) \times (1/r)$, the cloud liquid and cloud ice mixing ratios being unmodified. This changed the fraction of convective cloud to total cloud into that of the perturbed climate, while retaining in cloud liquid and ice water mixing ratios from the control. Finally, $\delta R_{\tilde{C}_T}$ was calculated by substituting $\tilde{T}'$ for $\tilde{T}$ during the determination of cloud optical properties, whilst restoring $\tilde{T}$ for the final radiation calculations. All water substance mixing ratios were retained unchanged.

The total perturbation to radiation due to all cloud changes can then be written, (assuming the changes are linear and independent) as

$$\delta R_{\tilde{C}} \approx \delta R_{\tilde{C}_A} + \delta R_{\tilde{C}_H} + \delta R_{\tilde{C}_W} + \delta R_{\tilde{C}_P} + \delta R_{\tilde{C}_C} + \delta R_{\tilde{C}_T} \ . \tag{18}$$

A test of the validity of these assumptions is provided in Sect. 3.

Fields substitution and radiative calculations were performed using instantaneous model output, archived every 21 model hours throughout the month to minimise any biases due to diurnal sampling.

The use of instantaneous fields avoids the complication that the total cloud cover from the monthly mean fields is different to the mean of the total cloud calculation from instantaneous (daily) cloud fields. Thus, for example, if mean fields are used the planetary albedo is altered, and some sort of scaling is needed to restore the original time average of the instantaneous total cloud amounts (e.g. Gong et al. 1994).

Furthermore, the time-averaged radiative impact of the (instantaneous) cloud changes cannot be accurately estimated using any field of time-mean clouds (e.g. Wetherald and Manabe 1988). Taylor and Ghan (1992) make the point that total top-of-atmosphere (TOA) albedo cannot be accurately estimated from the time mean of the total column liquid water path, as this mean is heavily biased towards the lower clouds (with high values of cloud liquid water).

Thus, it appears that quantitative feedback information may be inferred only from instantaneous substitutions. Unfortunately, the method of daily substitution has the disadvantage of being computationally extremely expensive. When investigating clear and cloudy changes in the present analysis, around 80 radiation calculations were performed (20 "fields" $\times$ 2 (clear/cloudy) $\times$ 2 (swapping control and perturbed)) for each pair of climate archives.

2.4 Validation of control climate

This section will briefly compare the control climate of the model with observations. It will concentrate on those fields which we may anticipate are important for model feedbacks. It should be borne in mind however, that agreement with observations in the present climate does not necessarily imply feedbacks are correctly modelled. Agreement with observations must therefore be regarded as a

necessary, although not sufficient, requirement for the accurate representation of feedbacks (Watterson et al. 1999).

Sea surface temperature and sea-ice extents and their annual cycles are in good agreement with observed values (not shown), as oceanic Q-fluxes and sea-ice bottom fluxes were prescribed to ensure this. Of more immediate importance for the feedbacks considered here are the distributions of water vapor and clouds, cloud liquid water, cloud forcing and precipitation.

Table 1 contains a comparison of model layer precipitable water with the NVAP observations, compiled by Randel et al. (1996). Overall the hemispheric and layer distributions are in good agreement with the observations, although southern hemisphere moisture values below 500 hPa and northern hemisphere moisture values above 500 hPa are both a little too large. Global annual mean total precipitable water is only around 7% greater then the observations.

Model high, middle and low cloud are compared with ISCCP (Rossow and Schiffer 1991), Warren et al. (1986, 1988) and Nimbus (Stowe et al. 1989) cloud observations in Colman (2001), (their Fig. 3). Overall the vertical and latitudinal variations of clouds compare quite well with the available observational data sets, particularly considering observational uncertainties. Readers are referred to that paper for further discussion.

Colman (2001) also compares TOA LW and SW with Earth Radiation Budget Experiment (ERBE) observations (Harrison et al. 1990). Those results indicate that the cloud forcing components agree well with observations overall. Agreement in both LW and SW are particularly good throughout the tropics and sub tropics. Consistent with this it is found that zonal OLR and planetary albedo also agree well with ERBE values (not shown). The main model shortcoming is a somewhat weak SW cloud forcing in the poleward portion of the circumpolar trough.

The seasonal change in cloud forcing can provide some test on how well the model simulates variations in clouds and the associated forcing (Senior and Mitchell 1993). For the LW, the calculation is a straightforward difference in cloud forcing between January and July and is shown for the model and ERBE in Fig. 1b. For the SW, seasonal changes in insolation dominate the variation in cloud forcing, and these must be removed to isolate the signal from cloud changes. Here this was done following Cess et al. (1997) (their Eq. 5) for each season and then calculating the difference. The results for SW are shown in Fig. 1a for model and observations.

The largest seasonal change in cloud forcing in the LW in the observations is at around 10°N and S, corresponding in a shift in clouds with the seasonal movement of the Inter Tropical Convergence Zone (Senior and Mitchell 1993). The magnitude of the seasonal cloud forcing change is well simulated in the model, although the actual latitudinal shift is slightly too large. Overall model agreement with observations is very good equatorward of mid latitudes. Poleward of this, disagreement is somewhat greater, with the observed peaks at around 60°N and 70°S not being picked up, although the latitude band 40–60°S shows fair agreement.

In the SW (Fig. 1a), overall agreement is very good between model and observations. The peaks at 10°N and S are well captured in location in the SW, although the magnitude of the cloud forcing change is slightly low. Agreement to 60°S and 50°N is very good overall, suggesting the model is simulating seasonal changes in mid latitude clouds as well. There is some suggestion, however, that cloud changes at 60°N are too great in the model.

Table 1 Annual mean layer precipitable water contents (in mm) for the model, and the NVAP observations (in brackets) from Randel et al. (1996). Shown are Northern and Southern Hemispheres (NH, SH), and global values

	NH (observed)	SH (observed)	GLOB (observed)
500–300 hPa	1.71 (1.5)	1.41 (1.4)	1.56 (1.5)
700–500 hPa	5.20 (5.0)	4.65 (4.2)	4.92 (4.6)
1000–700 hPa	19.8 (19.4)	19.8 (18.4)	19.8 (18.9)
Total	26.7 (25.7)	25.9 (23.3)	26.3 (24.5)

Overall the agreement between model and observations for LW and SW seasonal cloud forcing is good, although there is a suggestion of some model problems at high latitudes in the LW (and possibly also in the Northern Hemisphere in the SW).

As the present work considers in detail the cloud feedbacks due to liquid water changes, the simulated liquid water path is also compared with observations. Figure 2 shows a comparison of liquid water path (LWP) for the model, and for the satellite observations of Weng and Grody (1994). Zonal model distributions show reasonable corresponding peaks (Equator, 50°N and S) and troughs (subtropics) but the total water path is somewhat smaller than the observations at low-latitudes, and larger in mid latitudes. The observational LWP data of Greenwald et al. (1993) (not shown) over the ocean are higher than those of Weng and Grody (1994) over most latitudes. July values (not shown) show similar patterns, with model subtropical values being reasonable, although mid latitude peaks are again too large. Some of this latter bias is

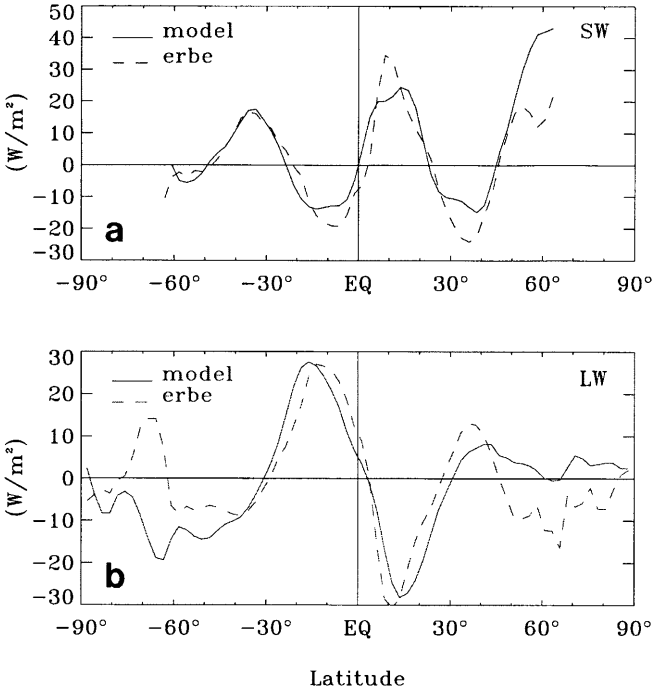

Fig. 1a, b Zonally averaged January-July cloud forcing at the TOA for the model (*solid line*) and ERBE (*dashed line*) in W/m^2. **a** cloud shortwave forcing (with seasonal change in incoming solar radiation removed, see text for details), and **b** cloud longwave forcing

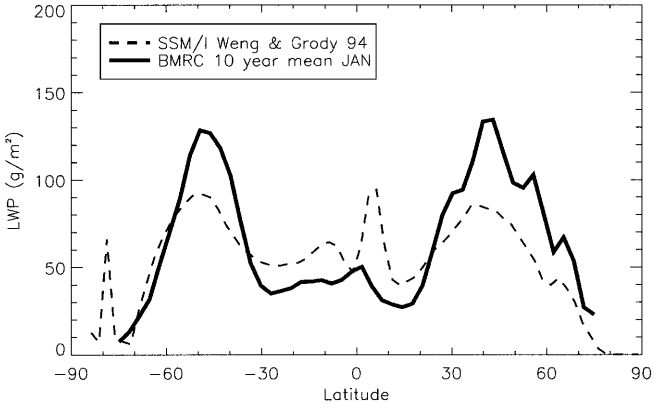

Fig. 2 January mean cloud liquid water path: model versus observations due to Weng and Grody (1994)

almost certainly the result of excessive low cloud amounts in the NH and SH storm tracks (see Fig. 3a in Colman 2001). Zonal precipitation patterns in January and July are also in good agreement with observations (not shown).

Overall, given the uncertainties in the cloud observations, the control climate moisture and cloud distribution and LWP appear to be reasonable as do the resulting cloud forcing, the seasonal change in cloud forcing and the precipitation. The following section will consider the diagnosed model feedbacks under climate perturbations.

3 Feedback results

3.1 Global feedbacks

This section will briefly describe the global feedbacks diagnosed from 10 years of data from the $1 \rightarrow 2xCO_2$ experiment for the BMRC model. Table 2 lists global values for LW, SW and total feedbacks, as well as their "clear sky" values. Also shown are total feedbacks, and the sum of all terms.

The strongest negative "feedback" (often thought of as the response without feedbacks) is that due to the surface temperature (T_*) response, and is equal to -3.2 W/m^2/K. This is close to the value of -3.3 W/m^2/K expected from simple black body emission arguments (e.g. Cess et al. 1990). The clear sky T_* feedback (Table 2) is stronger than the all sky value, as the presence of clouds raises the effective radiative height of the atmosphere above that of the cloud free value (McAvaney and Colman 1996), hence lowering emitting temperature.

Lapse rate (Γ) is the other negative feedback, and can be considered as further strengthening the cooling due to the surface temperature response. The Γ feedback is only

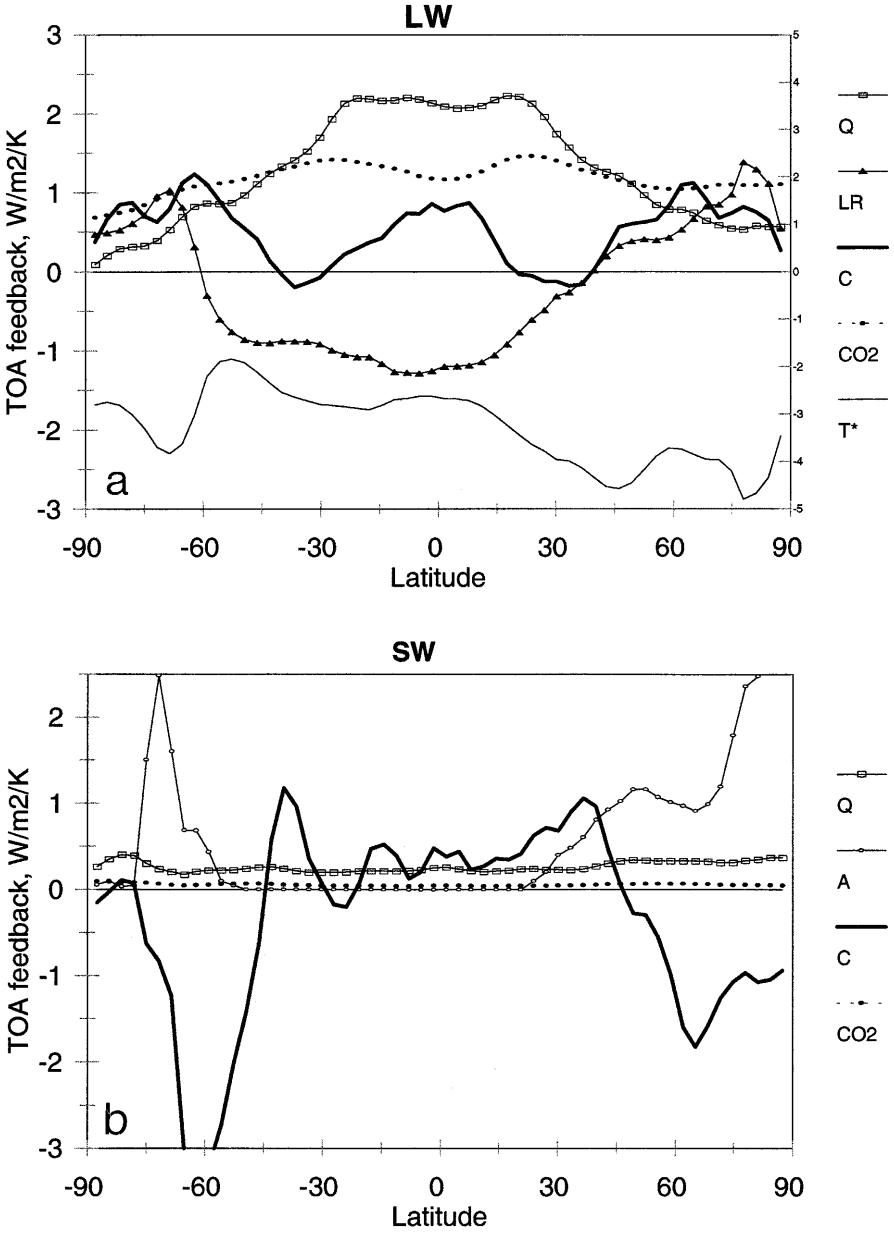

Fig. 3a, b Ten year zonal mean TOA feedbacks (W/m^2/K) for surface temperature (T_*), lapse rate (LR), water vapour (Q), surface albedo (A), clouds (C). Also shown is the CO_2 forcing, normalized by the change in surface temperature. Note that the T_* feedback is scaled differently from the other feedbacks, and refers to the right hand axis. Shown are **a** LW and **b** SW

Table 2 Global feedbacks (in $W/m^2/K$) for the BMRC model. Listed are separate longwave (LW) and shortwave (SW) components, as well as the total (LW + SW) and the total clear sky values. The sum of all feedback components ($\sum$) as well as the net feedback (All) are also shown. Cloud component feedbacks are also given. Refer to text for feedback definitions. Standard deviations (over 10 years) are specified in brackets. CO_2 forcing (in W/m^2) is also included

Feedback	LW	SW	LW + SW	Clear sky
T_*	−3.2 (0.092)	0	−3.2	−3.5
Γ	−0.54 (0.084)	0	−0.54	−0.51
q	1.59 (0.052)	0.24 (0.009)	1.84	2.28
q_A	1.04 (0.038)	0.22 (0.009)	1.26	1.58
q_H	0.56 (0.029)	0.031 (0.002)	0.59	0.70
C	0.43 (0.058)	−0.08 (0.13)	0.36	–
α	0	0.29 (0.037)	0.29	0.48
$\sum$	−1.72	0.46	−1.26	−1.25
All	−1.69	0.45	−1.24	−1.27
CO_2 (W/m^2)	3.43	0.14	3.57	3.73
C_O	0.56 (0.031)	−0.75 (0.029)	−0.19	–
C_F	−0.08 (0.061)	0.61 (0.12)	0.53	–
C_A	−0.14 (0.060)	0.31 (0.11)	0.17	–
C_H	0.066 (0.028)	0.30 (0.027)	0.37	–
C_W	0.49 (0.029)	−0.27 (0.014)	0.22	–
C_P	0.041 (0.001)	−0.53 (0.020)	−0.49	–
C_C	0	0.057 (0.006)	0.06	–
C_T	0.037 (0.002)	−0.044 (0.002)	−0.01	–

marginally affected by the presence of clouds globally in the present experiments. In contrast, Zhang et al. (1994) noted a strong cloud impact in fixed season, perturbed SST experiments.

By far the strongest positive feedback is that due to water vapour (q). Around 85% of this comes from the LW term. Clouds have a weakening impact of around 20%. The division of this feedback into amount and height terms is considered in the next section.

Cloud and albedo feedbacks are roughly equal. The cloud feedback is weakly positive in the LW, and close to zero in the SW. For the SW, the negative cloud optical property feedback is around $2\frac{1}{2}$ times the magnitude of the albedo feedback. It is, however, closely balanced by the positive cloud fraction feedback. In the present experiments the LW cloud fraction term is close to zero, but there is a strong, positive optical property feedback. These components, and their further subcomponents, are considered in more detail in the following section.

The surface albedo is found to be the strongest (net) SW feedback, although it is only slightly larger than the SW q term. What is notable from Table 2, however, is the important impact of clouds on this feedback, reducing its value by around 40% from the clear sky value (roughly in line with the findings of Ingram et al. 1989). The latitudinal details of this is also discussed in the next section.

Table 2 also includes the value of the feedbacks from all fields substituted simultaneously (''All'') as well as the sum of all individual feedback terms, except for cloud sub-components ($\sum$). These numbers agree to within around 2% for both LW and SW. This indicates that the ''double substitution'' method works extremely well for the evaluation of the individual feedbacks, and suggests further that the ''non-linear'' terms (e.g. feedbacks due to simultaneous changes due to two or more processes) are almost certainly small (see also Rotstayn 1999, Colman et al. 1997 for further discussion).

All global values are the results of 10 years of annual means. Also shown (in brackets) is the standard deviation of the feedback over the 10 years. This gives a measure of the interannual variability of the feedback, (and by implication how long an analysis we must run to accurately determine its value). Lowest (relative) interannual variability occurs for T_* and q feedbacks. Greatest variability occurs for cloud feedbacks. Subdividing the cloud feedback further reveals that cloud fraction (amount and height) feedbacks vary much more from year to year than do the optical property component terms. The variability is particularly large in the SW C_F term. One or two years of analysis is obviously insufficient to estimate this term accurately, even at a global scale.

3.2 Zonal feedbacks and feedback non-linearities

This section will consider the feedbacks (with particular emphasis on the cloud feedbacks) in the model in more detail, describing them as a function of latitude and dividing them, where possible, into contributing components, as well as determining the cloud impacts on individual feedbacks and examining their linearity under climate warming.

Figure 3a and b shows the zonal means of the main feedbacks for LW and SW respectively. Water vapour and cloud feedbacks are shown as totals, their sub components are considered separately below. Note that the TOA CO_2 forcing is included in Fig. 3, but has been normalized by the global mean surface temperature change, which permits a direct comparison of the TOA impacts of the forcing and resulting feedbacks in the one figure.

3.2.1 CO_2 forcing

The LW CO_2 forcing is weakly peaked in the sub tropics, although overall it is reasonably uniform with latitude in both LW and SW. The horizontal distribution of this forcing has a very similar regional pattern to that of Kiehl and Briegleb (1993) (not shown). Zonally the CO_2 forcing is similar to that of Le Treut et al. (1994) although note that in that reference the CO_2 forcing did not include the effects of stratospheric cooling as it does in the present case (see Hansen et al. 1981 for discussion of this point).

3.2.2 Water vapour

The strongest positive feedback, that of LW water vapour is strongly peaked in the tropics, with an extended, relatively flat maximum equatorward of 30° of latitude. Poleward of this it falls off steeply, dropping to half strength by around 45°. In polar regions it is small, falling to 1/4 tropical strength at the north pole, and close to zero at the south pole.

The SW water vapour feedback (see Fig. 3b) is, by contrast, much more uniform with latitude, indeed showing a slight increase in strength towards the poles. This increase appears to be the result of high surface albedo increasing the atmospheric path length, and hence the sensitivity to changing water vapour of the SW radiation (Colman 2001).

Allowing for area weighting, 2/3 of the global SW + LW q feedback strength is accounted for equatorward of 30°. The overall shape of the zonal q feedback profile in the present results is very similar to that of Le Treut et al. (1994, their Fig. 17). They, too, find a low-latitude dominance of their feedback, with tropical values again being around twice those at 45°. Their peak tropical values lie at around 3 $W/m^2/K$, 20% higher than those for the net (LW + SW) BMRC feedback.

The total water vapour feedback was further subdivided following the method of Hansen et al. (1984). The water vapour amount (q_A) feedback shows that part of the total which is due simply to increased total precipitable water in the atmospheric column. The height feedback (q_H) is that term resulting from changes in vertical distribution, analogous to the lapse rate feedback for temperature. Both theory and observations indicate that an upward shift in water vapour distribution for fixed precipitable water decreases upwards LW at the TOA (Stephens and Greenwald 1991). Thus a relative upwards shift in water vapour profile in a warmer climate would represent a positive feedback. Such a shift is indeed commonly found in GCM results (e.g. Watterson et al. 1999).

Figure 4a shows the zonal LW q_A, q_H and lapse rate (LR) feedbacks, including the clear sky terms (i.e. with clouds instantaneously removed for the feedback calculations). Both q_A and q_H feedbacks are positive at all latitudes, with q_A also being consistently the larger of the two. The largest relative contribution to total q feedback by the q_H component lies at low-latitudes, at around 40% of the net water vapour response in the zonal mean. This is consistent with an increase in tropical convection, and a maximum in global upper tropospheric warming, and consequent upwards shift in q (Colman 2001, Fig. 3a). Pollack et al. (1993) also divided their total q feedback into q_A, q_H terms (using a 2D RCM) and similarly found the q_H contribution to q to peak at low latitudes, also around 40–45%. However it is notable that the q_H feedback is positive at all latitudes, even near the poles where lapse rate increases occur in the warmer climate, as evidenced by negative LR feedback in Fig. 4a. This feature of the warmer climate, that upper level water vapour increases (proportionately) more than lower at all latitudes was also noted by Le Treut et al. (1994, their Fig. 11) and Colman and McAvaney (1997) for an earlier version of the BMRC model. Two reasons for such increased upper level relative moistening were suggested by Mitchell and Ingram (1992). Firstly, the fractional change in saturation vapour pressure decreases with temperature (following the Clausius Clapeyron relation), and hence increases with height. Secondly, at low latitudes the warming tends to increase with height (see next section).

The role of clouds in determining the strengths of water vapour feedbacks has only rarely been discussed in the literature. Indeed, the commonly adopted 'method II' means of evaluating clear sky feedbacks (Cess et al. 1990) expressly removes their impact, producing results probably more representative of a cloud free planet than of their true impacts in GCMs. Zhang et al. (1994) noted significant cloud impacts on water vapour feedback (reducing it by around 25%) and lapse rate feedback (up to doubling it) in fixed season perturbed SST experiments.

Zonal mean cloud fraction in the 1xCO_2 climate is shown in Fig. 5a. The impact of clouds on the LW water vapour feedback is illustrated in Fig. 4a, which shows both "clear sky" and "all sky" feedbacks. Both q_A and q_H LW feedbacks are weakened by clouds at all latitudes (Fig. 4a). Maximum reductions occur at low latitudes, consistent with the upper cloud maximum around the ITCZ. Overall the fractional reduction of q_A by clouds is greater than that of q_H (globally 30% compared with 20%). In a clear-sky world, then, the net LW q feedback would be even more dominated by the q_A component.

The SW q feedback (Fig. 4b), by contrast, shows an increase in strength with the addition of clouds. Detailed vertical analysis from an idealised increase in water vapour found that over most latitudes the feedback increase results from increased absorption of SW radiation in the layers above around 900 hPa, with a reduction close to the surface. Only at high latitudes does the addition of clouds reduce the feedback strength above the surface layer. Thus the impact of clouds (over low albedo surfaces) is to increase the SW absorbed, through the increase of atmospheric path lengths due to

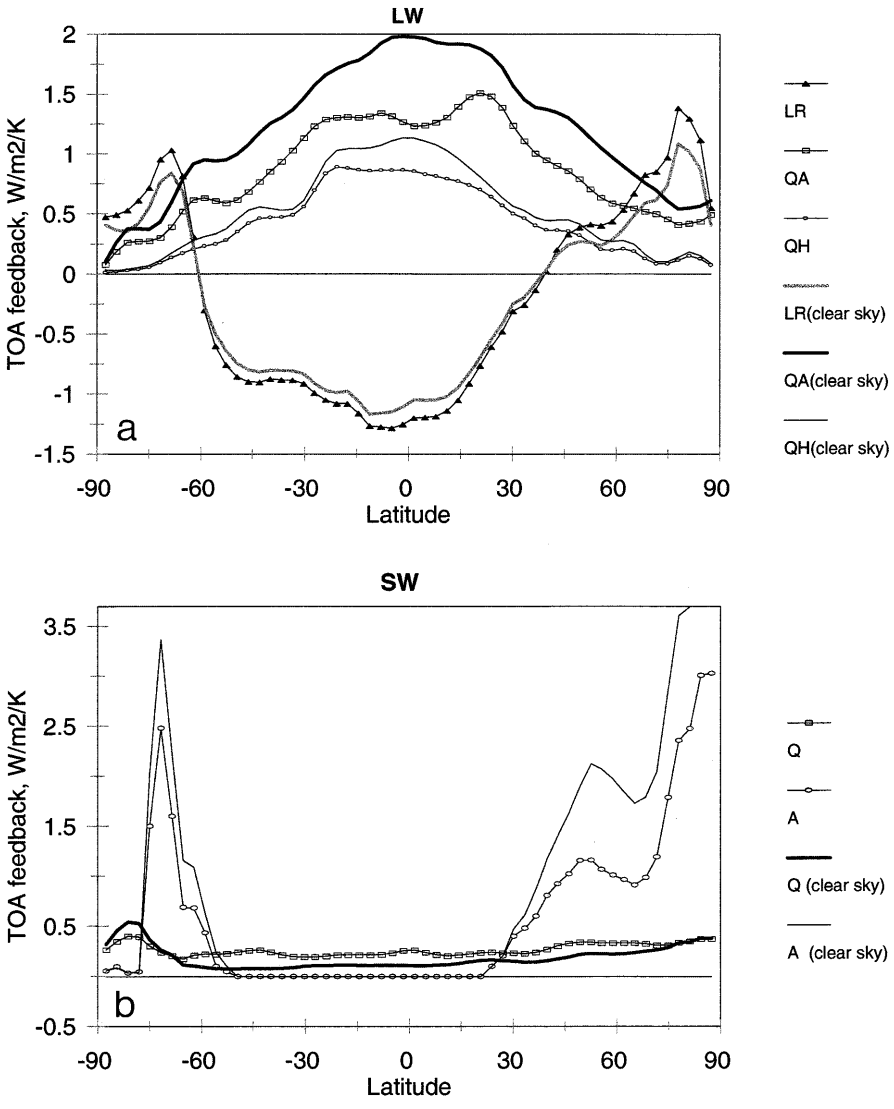

Fig. 4 a LW feedbacks ($W/m^2/K$) for lapse rate (LR), water vapour amount (QA) and water vapour height (QH), for clear sky and all sky calculations. **b** SW feedbacks ($W/m^2/K$), clear sky/all sky for albedo (A) and water vapour (Q)

cloud reflections. Zhang et al. (1994) found clouds to increase SW q feedback by around 50% for fixed season SST perturbations, roughly in line with the present findings.

To examine how robust (and also how non-linear) the model feedbacks are, they were also calculated between 2x and 4xCO_2 climates. Of course the climate forcing resulting from the $2 \rightarrow 4xCO_2$ change almost exactly matches that from the $1 \rightarrow 2xCO_2$ change due to the near logarithmic response of forcing to CO_2 concentration. The results are shown in Table 3 (showing the ratio of the two feedbacks).

Both q_A and q_H feedbacks are found to be only weakly non-linear over the full 4xCO_2 range of warming, with around 15% increase in strength for 2x to 4xCO_2 compared with 1x to 2xCO_2. Although this non-linearity is still relatively small it does indicate that there is a systematic increase in water vapour feedback strength with increasing global temperature. Indeed it is the principal reason why the model climate sensitivity increases slightly from 2x to 4xCO_2 (0.80 K m^2/W) compared with 1x to 2xCO_2 (0.77 K m^2/W), despite a marked weakening of the albedo feedback (discussed later). This weak non-linearity is reflected in the q_A and q_H feedbacks becoming slightly stronger at all latitudes (not shown). Peak absolute changes to the strength of the q components occur at low latitudes, however greatest fractional changes are at higher latitudes. For example, at 70°N, the q_A feedback at 2x to 4xCO_2 is nearly 50% stronger than at 1x to 2xCO_2 (although the global contributions of these latitudes remains small). At low-latitudes both q_A and q_H are around 15% stronger in the warmer climate, a value close to the global mean.

3.2.3 Lapse rate

The lapse rate feedback (see Fig. 3a) is the strongest negative feedback in the model with the exception of the

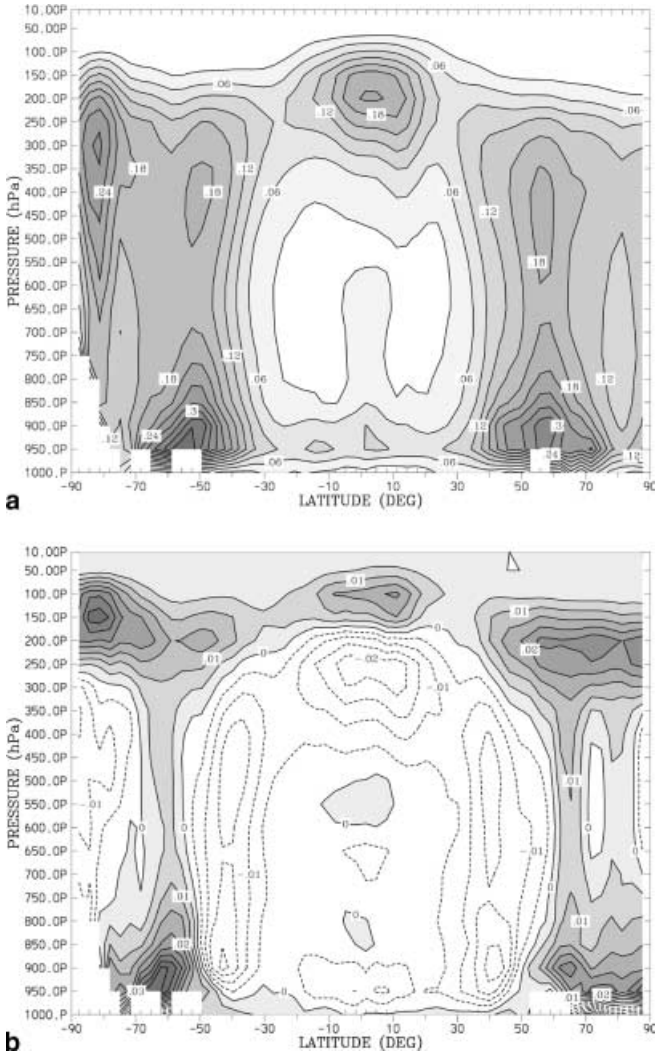

Fig. 5 a Zonal mean cloud fraction, $1xCO_2$ climate. Contour interval is 0.03. **b** Cloud fraction changes, $2xCO_2$ minus $1xCO_2$. Contour interval is 0.005

Table 3 Table showing the feedback strength in the $2 \rightarrow 4xCO_2$ climate change compared with that of the $1 \rightarrow 2xCO_2$ climate change (the former expressed as a fraction of the latter). Values which are different from unity at the 95% confidence level (over the 10 years of the analysed experiment) are shown in bold

Feedback	LW	SW	LW + SW
T_*	**1.04**	–	**1.04**
Γ	**1.15**	–	**1.15**
q_A	**1.12**	**1.04**	**1.10**
q_H	**1.18**	**1.11**	**1.18**
C	**1.25**	0.75	**1.36**
α	–	**0.63**	**0.63**
C_O	1.0	**0.94**	**0.80**
C_F	**−0.51**	0.97	**1.18**
C_A	**0.60**	0.88	1.11
C_H	**1.92**	1.07	**1.21**
C_W	1.0	1.01	0.98
C_P	**1.07**	**0.92**	**0.90**
C_C	–	1.10	1.10
C_T	1.01	1.04	1.20

surface temperature response itself. Negative values peak at low latitudes, corresponding with maximum lapse rate decreases associated with the maximum upper tropospheric warming universally found in $2xCO_2$ experiments. At low latitudes, surface LW emission is a maximum, further increasing the importance of the feedback in these regions. Positive values of lapse rate feedback occur at high latitudes in the Southern Hemisphere and mid to high latitudes in the Northern Hemisphere. At very high latitudes the positive LR feedback actually becomes larger than the water vapour contribution. Globally, however, the low-latitude negative regions provide the dominant contribution to LR feedback, resulting in a net negative value, comparable in magnitude to q_H (Table 2).

The pattern of low-latitude negative and high-latitude positive for the lapse rate feedback is similar to that noted by Pollack et al. (1993) and Gong et al. (1994), although the crossover in the present work occurs slightly further poleward in the Southern Hemisphere than that of Pollack et al. (1993).

The cloud impact on LR feedback (Fig. 4a) is of amplification of its magnitude (whether positive or negative) at all latitudes. A global amplification was found by Zhang et al. (1994) and was attributed by them to increased emissivity of a cloudy sky compared with a clear sky. Note however, that in the present experiments the effect of clouds is quite small, only increasing feedback strength by around 10%, compared with an approximate doubling found by Zhang et al. (1994). The present result is probably more credible, as the uniform SST perturbation method used by Zhang et al. (1994) is known to strongly distort the lapse rate feedback compared with that of a more "realistic" climate change (Colman and McAvaney 1997).

The lapse rate feedback is also weakly non-linear over the full range of warming to $4xCO_2$ (Table 3). In low latitudes it strengthens in a warmer climate, consistent with a non linear decrease in lapse rate (Colman et al. 1997) but the effect is not statistically significant at all latitudes (not shown).

3.2.4 Surface albedo

The albedo feedback (Fig. 3b) is the most important positive SW feedback in the BMRC model and the second strongest positive term overall. The double peak in the Northern Hemisphere consists of a maximum at around 50°N associated with snow retreat over Asia and North America, and a high latitude peak associated with sea ice loss. The global contribution of changes to snow over land in the present experiments was calculated, and is approximately 45%, similar to the earlier finding of Ingram et al. (1989).

The effect of clouds on the albedo feedback (Fig. 4b) is the strongest of any feedback, reducing it by around 50%. The percentage reduction in albedo feedback is close to uniform with latitude. The

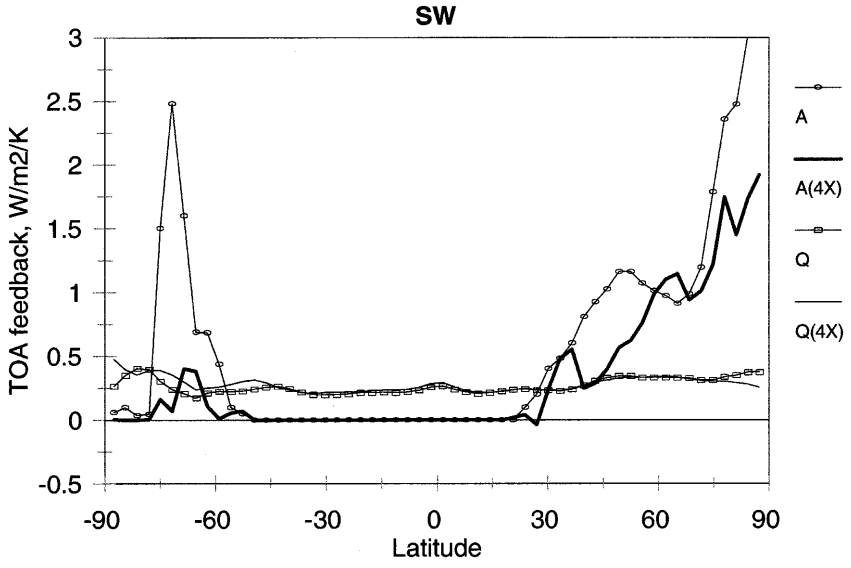

Fig. 6 SW $1 \rightarrow 2xCO_2$ and $2 \rightarrow 4xCO_2$ (labelled "*4X*") feedbacks for albedo and water vapour ($W/m^2/K$)

importance of clouds was noted by Ingram et al. (1989) and Le Treut et al. (1994). In the latter analysis a change in the cloud scheme resulted in a three fold increase in the albedo feedback. Peak values of Southern Hemisphere feedback strength from Le Treut et al. (1994) vary from 0.75 $\rightarrow$ 3.6 $W/m^2/K$. Peak values in the present experiments lie between these at 2.5 $W/m^2/K$. In the Northern Hemisphere the feedback is considerably stronger than that of both model versions used by Le Treut et al. (1994).

The albedo feedback is the most strongly non-linear of all feedback components in the model, decreasing globally by nearly 40% in the warmer climate (Table 3). The change in the zonal albedo feedback strength from $1 \rightarrow 2xCO_2$ to $2 \rightarrow 4xCO_2$ is shown in Fig. 6. Southern Hemisphere albedo feedback in the warmer climate (i.e. $2 \rightarrow 4xCO_2$) is particularly weak. There are two possible reasons for the decreases in feedback strength: reduced snow and ice cover, and increased masking by clouds.

Southern Hemisphere sea-ice cover in the 1, 2 and $4xCO_2$ climates (as a percentage of hemispheric area) is 6.5%, 4.2% and 2.5%. The reduction in area is more than one third greater for $1 \rightarrow 2xCO_2$ than for $2 \rightarrow 4xCO_2$ despite the smaller global temperature increase. An examination of the clear sky albedo feedback reveals a 25% reduction in the warmer climate, compared with the 38% reduction for the all sky feedback. This indicates that the masking of the albedo feedback does in fact increase as the climate warms (consistent with increased high-latitude cloud cover). This extra masking contributes about 1/3 of the total reduction in feedback strength. The other 2/3 is directly attributable to the clear sky component (i.e. to the decreased snow and sea-ice cover). Overall the present results are consistent with findings elsewhere that $2xCO_2$ sensitivity tends to increase with increased snow and sea-ice cover in the control climate (Washington and Meehl 1986).

3.2.5 Clouds

Figure 7 shows the latitudinal cloud feedbacks for LW and SW, for total, and for each of the components listed in Eq. (18). Clearly the final cloud feedback is a complex sum of contributing factors with differing processes being important at different latitudes. A test for how well the components sum to the total was made by evaluating both sides of Eq. (18). The results for the 10 year mean are shown in Fig. 8, and indicate that, indeed, the method of separation of cloud optical and fractional feedbacks works extremely well at all latitudes, and in both the LW and SW.

Cloud fraction changes from $1 \rightarrow 2xCO_2$ are shown in Fig. 5b. They indicate a pattern of general decreases equatorward of 50°, with marked increases at 60–70° in each hemisphere. The low-latitude decrease is manifest as a widespread reduction in all but the very highest clouds. Thus, total cloud amounts decrease, but the mean cloud height is increased. Patterns of cloud change qualitatively similar to this have been found in many $2xCO_2$ climate model studies (e.g. Mitchell et al. 1989; Wetherald and Manabe 1986; Le Treut et al. 1994). The high-latitude increase is partially the result of a slight poleward shift in the storm tracks, with an associated shift in maximum cloudiness.

The low-latitude cloud amount decrease produces a positive SW but a negative LW C_A feedback. At high latitudes, the situation is reversed. Indeed, the cloud amount feedbacks shown in Fig. 7a, b oppose each other at most latitudes, with the SW term being roughly twice that of the LW. The reason for this opposition is straightforward: a change in total cloud fraction (with fixed vertical cloud distribution), will produce opposing LW and SW radiation effects (Colman 2001). A decrease in cloud amount generally leads to a positive (negative) SW (LW) feedback, due to the negative SW (positive LW) cloud forcing (Ramanathan et al. 1989). Indeed, this compensating LW/SW response may lie behind

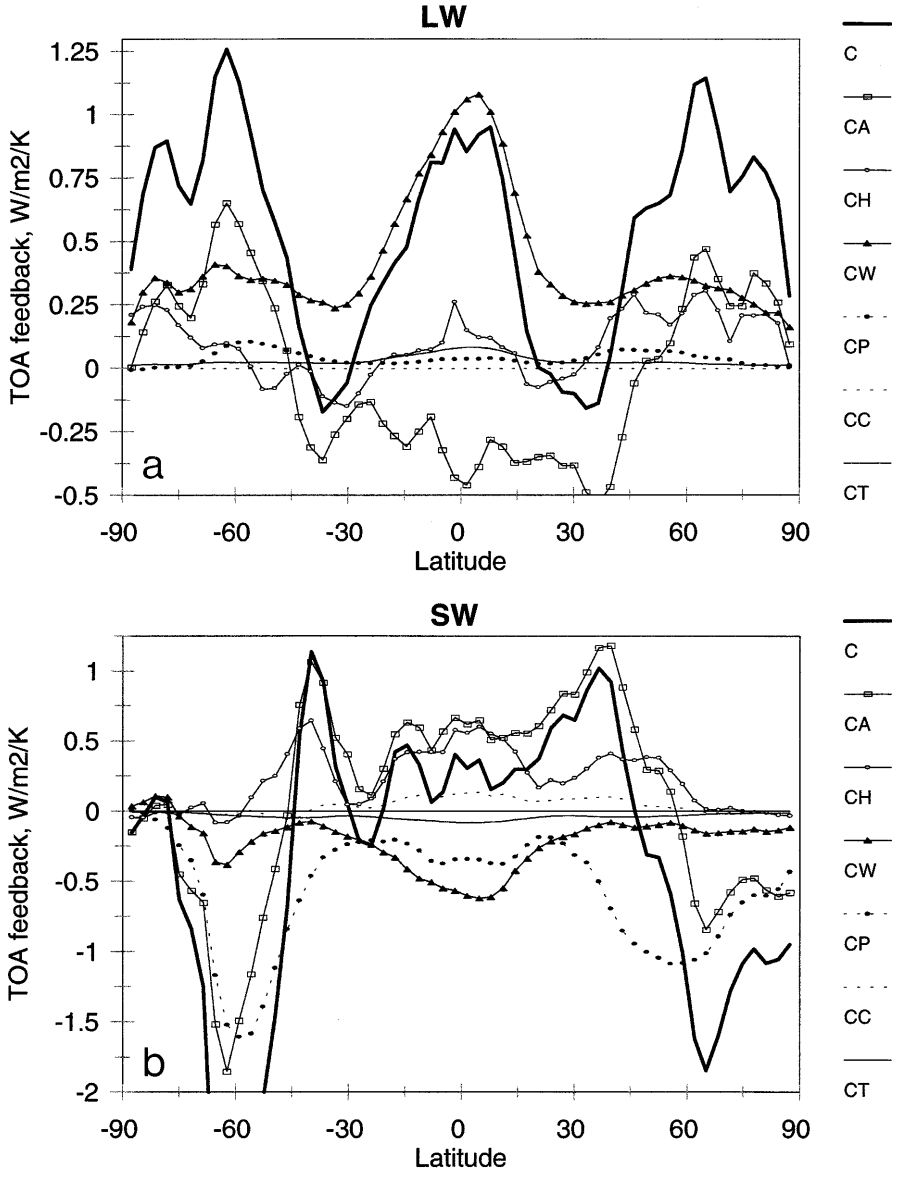

Fig. 7a, b Cloud component feedbacks (W/m^2/K) for **a** LW and **b** SW showing terms due to: cloud amount (C_A), cloud height (C_H), cloud water substance (C_W), cloud water phase (C_P), convective cloud amount (C_C) and cloud physical thickness (C_T). Also shown is the total cloud feedback (C)

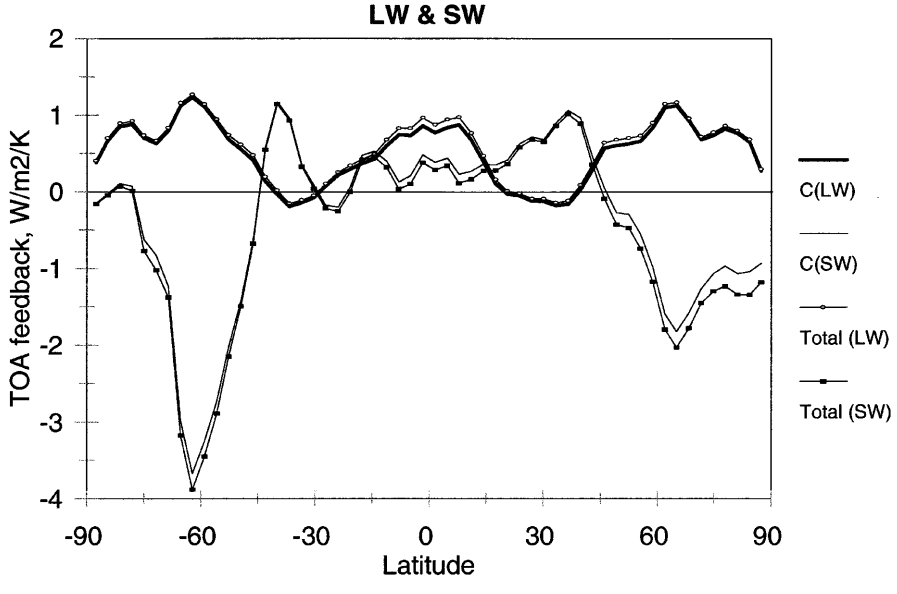

Fig. 8 Comparison of net cloud feedback (C) with sum of component terms ($C_W + C_P + C_C + C_T + C_F$) denoted as "*total*", for LW and SW (W/m^2/K)

some of the relative insensitivity of the net cloud feedback to parametrisation changes noted in some GCMs (e.g. Rotstayn 1999; Yao et al. 1999).

The LW cloud height feedback is positive at low latitudes, consistent with the upward shift in high clouds apparent in Fig. 5b. This feedback is quite weak however, particularly compared with previous model versions (Colman et al. 1997). The differences between those results and the present are consistent with the variation of emissivity and albedo with height in the current cloud parametrisation, a feature absent in the previous model version. Zonal mean ice cloud emissivity (in the $1xCO_2$ climate) is shown in Fig. 9. Tropical high cloud emissivity decreases rapidly with height above about 400 hPa, opposing the positive feedback from the increased height of the cloud which is particularly marked in this region. At high latitudes this emissivity/height gradient is reduced, and the LW cloud height feedback is more strongly positive (Fig. 7a).

For the SW, liquid and ice cloud albedo similarly decreases with height (not shown), producing a positive feedback as clouds form higher in the troposphere in the warmer climate. The C_H feedback is positive at almost all latitudes for the SW, with largest values tending to be in the tropics (Fig. 7b). A previous version of the BMRC model, with fixed cloud optical properties found a negligible SW C_H term (Colman et al. 1997).

A comparison may be done of the present results with the only other published values of zonal C_A and C_H feedbacks, those of Wetherald and Manabe (1988), their Fig. 14. The overall zonal patterns of Wetherald and Manabe (1988) are quite similar to the present, with low-latitude positive (negative) SW (LW) C_A feedbacks, with sign changes at higher latitudes (poleward of around 40°). Maximum tropical values in Wetherald and Manabe, $\sim$0.85 W/m^2/K for SW and $\sim$0.4 W/m^2/K for LW are quite similar to the present magnitudes. Cloud height terms are also quite similar in pattern and magnitude to the present. The latitudinal distribution of cloud feedbacks appears to be similar in the two experiments since the zonal pattern of cloud changes of Wetherald and Manabe (1988) resembles that of Fig. 5b, although not too much should be made of the rough agreement in the magnitude of the feedbacks themselves.

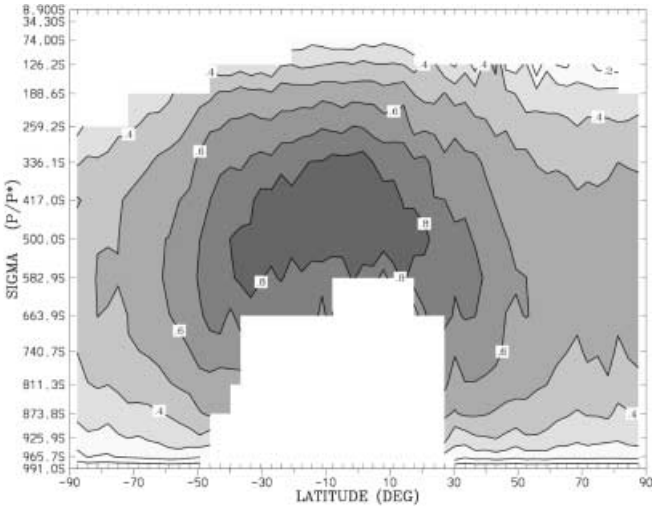

Fig. 9 Model ice cloud emissivity, $1xCO_2$ climate, January. Contour interval is 0.1

As the climate continues to warm past $2xCO_2$, the question arises as to whether cloud amount/height feedbacks might become more important due to non-linear cloud changes (as found for an earlier version of the model by Colman et al. 1997). For the SW both C_A and C_H feedbacks are reasonably linear (Table 3) as is the net C_F response. For the LW however, the C_A term weakens and C_H strengthens substantially in the warmer climate. Indeed, these impacts are sufficient to change the sign of the net C_F feedback between $1 \rightarrow 2xCO_2$ and $2 \rightarrow 4xCO_2$ (Table 3). Although the LW C_F term is only a minor contributor to net C feedback overall, this sign change does induce substantial non-linearity into the C feedbacks as the climate warms up to $4xCO_2$. This part is discussed further later.

The cloud component feedbacks making up the cloud optical property feedback (C_O) are shown in Fig. 7. Globally, the warmer climate is marked by an increase in cloud water substance. The overall cloud liquid water path increases 6% under a doubling of CO_2 (despite a small reduction in total cloud). At the same time, the fraction of cloud water which is frozen declines: from 44% of total water, to 42%.

The LW C_O feedback is dominated by C_W at all latitudes (Fig. 7a), i.e. by the change in total water substance within the clouds. The zonal mean distribution of in-cloud water content in the control ($1xCO_2$) climate is shown in Fig. 10a. The change in in-cloud water ($2xCO_2$ minus $1xCO_2$) is given in Fig. 10b. The change reveals that increases occur for clouds lying above an arc reaching from the surface at mid latitudes to around 600 hPa in the tropics with mainly decreases below this. The decrease in low level cloud water content with increasing temperature at low to mid latitudes is consistent with model and observational findings noted by Tselioudis et al. (1998), and was there attributed to an increase in the efficiency of precipitation processes in the warmer climates. Larger in-cloud water contents (ice or liquid) will increase emissivity (Eqs. 1, 4, 7, 8), and produce a climate warming in the LW. Only the upper cloud changes are important in the LW (Colman 2001), and hence only the increases in cloud water significantly affect the LW feedback, i.e. the low-lying regions of cloud water decrease have little LW impact. The maxima in C_W in the tropics, and at 60°N and S largely reflect the maxima in upper cloud fraction in these regions (Fig. 5a).

A change from ice to water cloud will also produce larger optical depths, and a positive LW feedback. Figure 11a shows the fraction of clouds which are composed of ice in the $1xCO_2$ climate. Figure 11b gives the change in this fraction going from the $1xCO_2$ to the $2xCO_2$ climates. Figure 11b reveals that there are

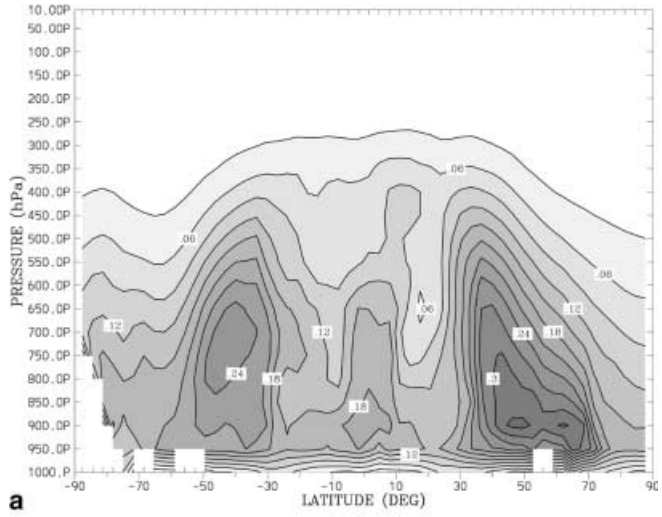

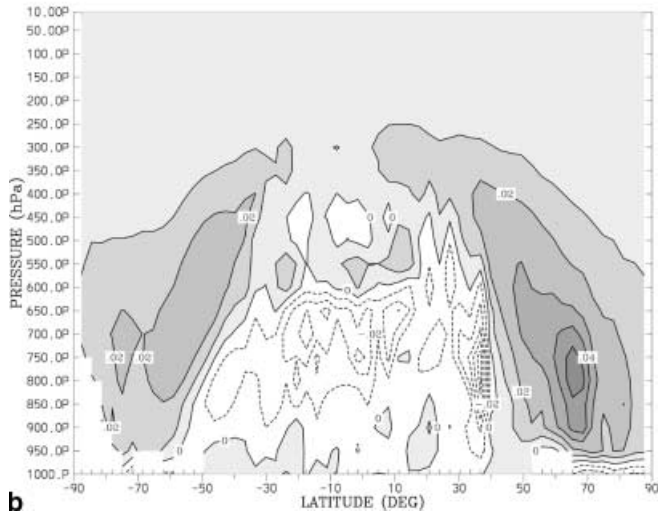

Fig. 10 **a** Annual mean in-cloud total water (i.e. liquid + ice) content (g/m^3) for the $1xCO_2$ climate. Contour interval is 0.03 g/m^3. **b** As **a**, but for $2xCO_2$ minus $1xCO_2$. Contour interval is 0.01

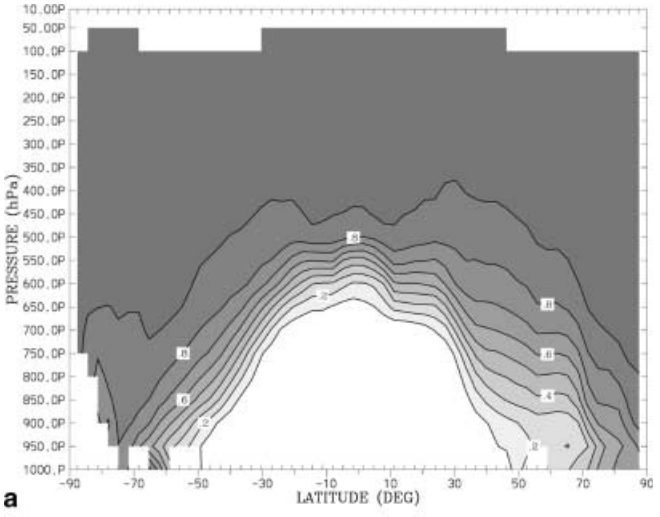

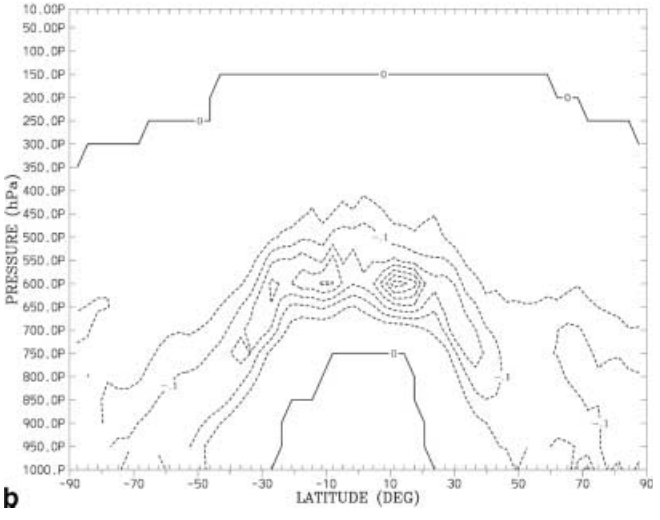

Fig. 11 **a** Annual mean fraction of clouds composed of ice for the $1xCO_2$ climate. Contour interval is 0.1. **b** As **a**, but for $2xCO_2$ minus $1xCO_2$. Contour interval is 0.05

decreases in the fraction of clouds composed of ice everywhere in the warmer climate with the largest decreases lying in an arc, close to the freezing level in the control (not shown). Significantly however, for LW feedback, very little change occurs in cloud phase above 400 hPa at any latitude. Thus the C_P LW cloud feedback is consequently weak (although positive) at all latitudes (Fig. 7a). This is not surprising: high, cold clouds would not be expected to contain large liquid water contents, even in a $2xCO_2$ climate. In fact, an examination of the $4xCO_2$ LW feedbacks (Table 3) shows only a small increase in the C_P term even at that degree of warming.

In contrast, in the SW, both C_W and C_P terms contribute significantly to the C_O feedback. At mid to high latitudes C_P is the dominant effect, as low to mid tropospheric ice clouds change to liquid clouds in the warmer climate (Fig. 11b), a negative feedback. The mid latitude contribution is particularly large as the regions of maximum phase change correspond with those of substantial (low level) cloud fraction and the warming there is large. In the tropical mid troposphere, cloud fractions are quite small (Fig. 5a) and so the SW C_P feedback is not particularly strong at low latitudes (although it is still positive). Senior and Mitchell (1993) similarly concluded that their phase change feedback had most contribution from low, mid latitude clouds, with a much smaller tropical component.

The SW C_W feedback is also negative (except over Antarctic latitudes), and is the major term in C_O at low latitudes. Increases in in-cloud water occur throughout the depth of the troposphere poleward of mid latitudes (Fig. 10b). Equatorward of this, the overall pattern is one of decreases below about 600 hPa, with increases above. Close to the surface, a mixture of increases and decreases is found. Important factors affecting the strength of the SW C_W feedback are the cloud fraction in the control (Fig. 5a), the water content in the control (Fig. 10a) and the strength of the incoming SW radia-

tion (the equatorial flux being around twice that at 70° latitude in the annual mean). The importance of the control climate in-cloud water content can be seen from Fig. 12. This shows cloud albedo as a function of cloud liquid (ice) path for water (ice) clouds 1 km thick at 850 hPa (250 hPa). For both liquid and ice clouds a given increase in cloud water content will have a greater impact on albedo if the water content is small in the control, than if it is large. Optical properties in the present scheme are calculated following Slingo (1989) for liquid water clouds. A comparison of the present optical properties with a number of other cloud optical property parametrisations (Sun and Shine 1994; Lemus et al. 1997) are included in Fig. 12 and all three display a similar "plateauing" of albedo with high values of cloud liquid water.

In the tropics, typical low level in-cloud water contents are around $0.15 \rightarrow 0.2$ g/m^3 (Fig. 10a). A 1 km thick cloud in these levels would have a liquid water path of $150 \rightarrow 200$ g/m^3, making its albedo relatively insensitive to liquid water changes (Fig. 12). Consistent with the present results, Senior and Mitchell (1993) found relatively small changes in low cloud albedo under climate warming despite general decreases in cloud liquid water mixing ratio at low latitudes. With increased height, control climate liquid water contents decrease and sensitivity to changes increases. Thus above 600 hPa in the tropics, where general liquid water increases occur, typical control climate in-cloud water contents are below 0.1 g/m^3.

Above about 450 hPa the cloud ice fraction is greater than 90% (Fig. 11a) and the ice cloud relationship of Fig. 12 characterises the albedo response. Although the ice cloud albedo curve is generally less steep than that of liquid for a given water path, typical in-cloud water paths in the upper troposphere are very low in the model (< 0.03 g/m^3 above 300 hPa) which increases sensitivity.

Control cloud fraction also plays a major role in the feedback. Between 650 and 850 hPa in the tropics and sub tropics, where in-cloud water content decreases are at their greatest, cloud fractions are small (Fig. 5a), which weakens the contribution to the C_W feedback. On the other hand, in the upper troposphere at these latitudes, where in-cloud water contents increase in the warmer climate, cloud fractions are substantially greater and the feedback is enhanced.

The net effect at low latitudes, then, is a negative SW C_W feedback, peaking around the equator (Fig. 7b). At mid to high latitudes large control climate in-cloud water contents and decreasing insolation with latitude mean that the feedback is somewhat weaker than in the tropics, although it remains positive everywhere (except over the Antarctic). A secondary peak is found at around 60°S (where cloud fractions are particularly large).

The remaining contributors to cloud optical property feedbacks, C_C and C_T, are both relatively small in the present experiments. In the LW, C_C feedback is zero (as emissivity is unaffected by the fraction of cloud that is convective). In the SW, C_C feedback is positive at all latitudes, peaking in the tropics. This is the result of an increase in convection, compared with large-scale condensation in the warmer climate, a change commonly found in GCMs (e.g. IPCC 1990). With the relative increase in convection, for a given amount of global cloud the albedo is lower, leading to increased net downwards SW at the TOA. In the tropics where convective increases are largest the magnitude of this feedback is around half that of the C_W term; but globally averaged its contribution is smaller, at around 25% of the magnitude of C_W (Table 2).

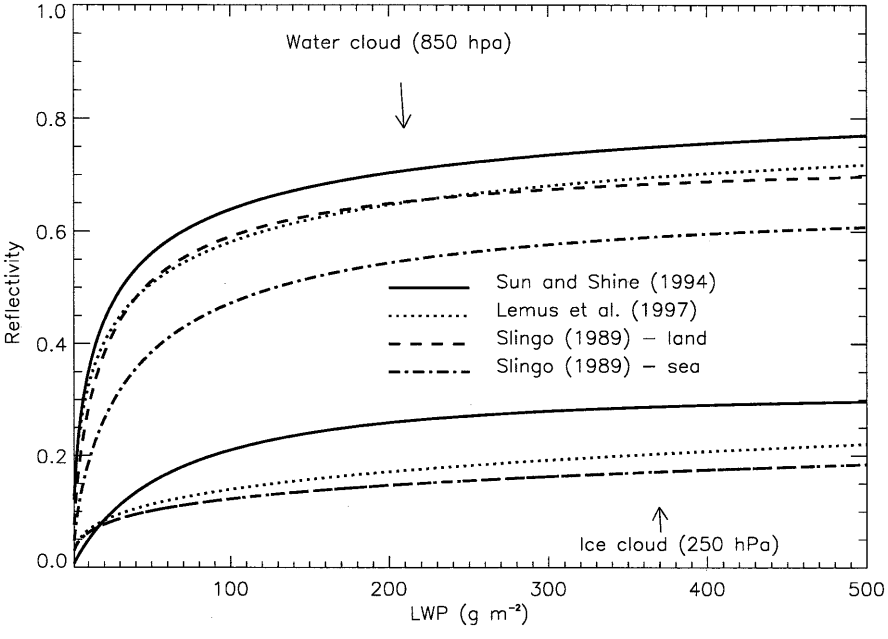

Fig. 12 Water and ice cloud albedo as a function of cloud (liquid or ice) water path (g/m^2) for a range of cloud optical property schemes. Refer to text for references (cloud thickness assumed to be approximately 1.0 km)

An important caveat on the C_C feedback term is that in the present cloud parametrisation, convective cloud amount is related directly to convective precipitation rate. Since increases in mean convective precipitation rates occur almost universally in global warming simulations (including the present one) this tends to "build in" an increase in convective cloud fraction in the warmer climate and hence a positive feedback. However, it remains possible that convective cloud fraction decreases could occur, despite the precipitation increases, since, for example, marked increases in saturation vapour pressure also occur in the warmer climate. Thus uncertainties remain on the C_C feedback in the present model, although its contribution to total cloud feedback was found to be small in these experiments.

The remaining feedback term, C_T, represents the cloud feedback resulting from changes in the physical thickness of clouds, due to changes in temperature. As the troposphere warms, air density decreases, and model clouds (assumed to fill one or more model levels) become slightly thicker. For ice clouds this increases the optical depth (combining Eqs. 1 to 3). The effect on LW and SW radiation of this effect is relatively small (but non zero). As expected, the C_T feedback is positive (negative) for the LW (SW), as thicker clouds have higher emissivity (albedo). Maximum values occur in the tropics, and are fractionally stronger in the SW than the LW (although largely compensating between the two).

The interannual variability of the cloud component feedbacks may be gauged from the standard deviations, shown in brackets in Table 2. Variability (relative to the magnitude of the feedback) is in general much larger for cloud component feedbacks than for the non-cloud feedbacks. Thus, for example, a single year of analysis yields reasonably accurate values for zonal water vapour feedback, but may be highly unreliable for cloud component changes. Within the cloud components, largest relative variability is found in the C_F components, C_H and C_A. Easily the largest absolute value of interannual variability is for C_A in the SW (this latter term making an important contribution to final C feedback). The optical property feedbacks, by contrast, are far more consistent from year to year.

Finally the question arises as to how net cloud feedback may change as the climate forcing continues past $2xCO_2$ to $4xCO_2$. In the BMRC model, between $1 \rightarrow 2xCO_2$ and $2 \rightarrow 4xCO_2$ the total cloud feedback strengthens by 36% (Table 3). An examination of Tables 2 and 3 reveals this to be due mostly to the LW feedback strengthening, as the net SW cloud feedback is relatively small throughout. Considering the LW cloud feedback in the $1 \rightarrow 2xCO_2$ change, it is dominated by the C_O term, and the C_F term is relatively unimportant. In going to $4xCO_2$ however, the C_F response is highly non-linear which results in a substantial non-linear change in the final C feedback. This non-linearity results from the LW C_F feedback changing from small and negative (for $1 \rightarrow 2xCO_2$) to small and positive (for $2 \rightarrow 4xCO_2$) due to more positive C_A and C_H terms in the warmer climate. On the other hand the LW C_O feedback component is almost exactly linear, since the dominant C_W component is itself linear up to $4xCO_2$.

4 Conclusions

The offline radiative perturbation method has been used to perform an extensive analysis of TOA radiation feedbacks in the BMRC climate model. The global net feedbacks were initially divided into terms due to the surface temperature, T_* (strictly the response "without feedbacks") lapse rate, (Γ), water vapour (q), cloud (C) and surface albedo (α).

In order of decreasing global importance the strongest positive feedbacks were found to be those due to water vapour, albedo and clouds. Of these q is by far the strongest term. Its three strongest components were the LW q_A, and q_H feedbacks followed by the SW q_A term. Each of these components contributes roughly double the next term to the net q feedback.

Strongest negative feedbacks were those due to surface temperature (T_*), lapse rate (Γ) and cloud optical properties (C_O). This last term was found to be the relatively small result of much larger offsetting positive (LW) and negative (SW) components.

The impact of clouds on non-cloud feedbacks was determined. The importance of this is that it quantifies the (direct) role of the cloud on these feedbacks, and suggests which might be most sensitive to, for example, changes in cloud parametrisations leading to cloud cover changes in the "control" climate.

With the exception of the lapse rate term, clouds reduce the strength of model feedbacks. In the present experiments clouds were found to reduce clear sky T_*, q and α feedbacks by approximately 10%, 20% and 40% respectively. Lapse rate feedback is increased by around 10% (although being negative, this also decreases global climate sensitivity).

The net result is, then, that for a given radiative forcing in the GCM, a larger control climate global cloud cover (assuming no changes to horizontal and vertical distribution) acts to decrease positive feedbacks, increase negative feedback (apart from that of the surface temperature response) and hence decrease overall climate sensitivity.

Localised differences in model control climate cloud cover (particularly in tropical upper cloud, and low cloud over snow and ice) of course may have proportionally much larger impacts for a given change.

Globally (and generally latitudinally also) the model feedbacks were mostly found to be only weakly non-linear under increasing CO_2 levels up to $4xCO_2$. Note, of course, that since the radiative forcing varies as close to the log of the CO_2 concentration, the $1 \rightarrow 2xCO_2$ and $2 \rightarrow 4xCO_2$ perturbations provide almost identical radiative forcings. As regards the feedbacks, between $1 \rightarrow 2xCO_2$ and $2 \rightarrow 4xCO_2$ the greatest impacts on

feedback strength were on α (37% decrease) and total cloud feedback (36% increase). Cloud optical feedbacks were almost completely unchanged in the warmer climate for the LW component, but weakened marginally in the SW. Both Γ and q showed a 15% strengthening.

The importance of the reasonable degree of linearity, particularly of the strongest feedbacks is twofold. Firstly, it demonstrates that the changes in model fields, as well as the radiation responses to them are generally fairly robust across the full range up to $4xCO_2$ warming. Thus, processes highly non-linear locally (e.g. due to changes in cloud cover or cloud water contents) do not translate into dominating global non-linearities. Of course, some possible coupled non-linearities due to ocean/atmosphere/sea-ice interactions which may operate are suppressed in the present study because of the simplified ocean and sea-ice components.

The second point is that the magnitude of the non-linearities give some indication of the error in feedback strength which results simply from biases in the model control climate (although *not* from errors in the parametrisations themselves). Thus, for example, the albedo feedback is obviously sensitive to changes in the amount of sea ice in the "control" climate. The water vapour appears to be much less so (a roughly 160% increase in water vapour occurs in the tropical upper troposphere from $1 \rightarrow 4xCO_2$, but water vapour feedback for $2 \rightarrow 4xCO_2$ is only 15% stronger than for $1 \rightarrow 2xCO_2$).

The method of feedback analysis was also extended in the present study, to calculate in detail the changes in cloud fraction and optical properties which made up the net cloud feedback. The cloud fraction feedback was divided in turn into feedbacks due to cloud amount (C_A) and height (C_H); optical property feedbacks into terms due to water content (C_W), water/ice fraction (C_P), convective cloud fraction (C_C) and physical cloud thickness (C_T). A division of this nature has not hitherto been possible from the methods of feedback diagnosis available for GCM results.

Of the major components (C_A, C_H, C_W and C_P), all but C_H produce LW/SW feedbacks of conflicting sign, with the result that confidence in the final net cloud feedback, C, becomes low. In the warmer climate, total cloud cover was reduced, mean cloud height was increased, cloud water substance was increased, cloud fraction of ice was reduced, the relative amount of convective cloud was increased and mean cloud thickness was increased. Although these changes are physically plausible (IPCC 1990, 1995), the present results are of course for only a single model, and substantial differences may occur in other models, and different SW/LW responses may occur.

Some general conclusions, however, may be made regarding the factors responsible for large cloud component feedbacks in the present model, which may be of more general applicability. Such component feedbacks were sensitive to:

1. The cloud fraction present in the location of change. Feedbacks due to changes in cloud height, water content and water phase are larger in regions with greater cloud amounts in the control climate. Thus, for example, SW phase-change impacts are much stronger in the storm tracks than in the tropical mid troposphere despite widespread phase changes in both regions.

2. The height at which the changes occur. Longwave feedbacks are sensitive almost exclusively to upper level changes (where the surface/cloud temperature contrast is greatest). Thus, for example, LW C_P feedback is weak in the tropics, despite widespread phase changes, because those changes occur too low in the atmosphere to have significant LW impact. Most SW components, on the other hand are sensitive across a range of levels. Cloud amount sensitivity for the SW however, is a maximum for low cloud as cloud albedo generally decreases with height.

3. The latitude of the change, it is apparent that both SW and LW cloud change impacts are largest at low-latitudes for a given change. TOA SW (LW) radiation falls off by around 60% (33%) from the equator to the pole. Clearly however, the factors producing feedback strength are far more complex. Thus, for example, SW q_A feedback is large at higher latitudes due to path length increases associated with high albedo surfaces.

4. The sensitivity of optical properties to changes in liquid/ice content. For a given perturbation to cloud water, the strength of the water content feedback is stronger in regions where cloud water/ice contents are low in the control climate (as optical thickness then varies more rapidly with water content). Thus, for example, the SW tends to be more sensitive to a given change in cloud liquid water in the upper rather than the lower troposphere.

5. The cloud height feedback is sensitive to the vertical gradient in optical properties. In particular, the LW feedback tends to be weaker where the gradient in optical thickness is large (e.g. in the tropical upper troposphere in the GCM) than where it is weak (the extra tropical upper troposphere). The opposite is true for the SW feedback.

6. Convective cloud fraction changes and cloud physical thickness feedbacks appear to be quite weak. (Note that a caveat remains on the C_C feedback due to the linking of convective cloud fraction to convective precipitation rate in the present model.)

The offline radiation perturbation, as applied here, proves to be a powerful tool for evaluating the processes responsible for final GCM sensitivity in a single GCM. The magnitude of each feedback, and the plausibility of their attendant physical processes must serve as the basis for quantifying our level of confidence in the final climate sensitivity. The present study is one step towards quantifying that uncertainty. The performance of feedback analyses on other GCMs would help to further quantify these uncertainties.

Acknowledgements The authors wish to thank John Mitchell, Lawrie Rikus, Richard Dare and an anonymous reviewer for comments which greatly improved the paper. Thanks to Louise Wilson and Zhian Sun for assistance with the figures. Thanks also to Lily Gao, Lucy Sandercock and Mary Purcell for typing. This work was supported by the Australian Greenhouse Office.

References

Arking A (1991) The radiative effects of clouds and their impact on climate. Bull Am Meteorol Soc 71: 795–813

Betts AK, Harshvardhan (1987) Thermodynamic constraint on the cloud liquid water feedback in climate models. J Geophys Res 92: 8483–8485

Cess RD and co-authors (1990) Intercomparison and interpretation of cloud-climate feedback processes in nineteen atmospheric general circulation models. J Geophys Res 95: 16 601–16 615

Cess RD and co-authors (1996) Cloud feedback in atmospheric general circulation models: an update. J Geophys Res 101: 12 791–12 794

Cess RD and co-authors (1997) Comparison of the seasonal change in cloud-radiative forcing from atmospheric general circulation models and satellite observations. J Geophys Res 102: 16 593–16 603

Colman RA (2001) On the vertical extent of atmospheric feedbacks. Clim Dyn 17: 391–405

Colman RA, McAvaney BJ (1997) A study of GCM climate feedbacks from perturbed SST experiments. J Geophys Res 102: 19 383–19 402

Colman RA, Power SB, McAvaney BJ (1997) Non-linear climate feedback analysis in an atmospheric GCM. Clim Dyn 13: 717–731

Gong W, Zhou X, Wang WC (1994) A diagnostic study of feedback mechanisms in greenhouse effects simulated by NCAR CCM1. Acta Meteorol Sinica 8: 270–282

Greenwald TJ, Stephens GL, Vonder Haar TH, Jackson DL (1993) A physical retrieval of cloud liquid water over the global oceans using special sensor microwave/imager (SSM/I) observations. J Geophys Res 98: 184771–18489

Hansen JE, Johnson D, Lacis A, Lebedeff S, Lee P, Rind D, Russell G (1981) Climate impacts of increasing carbon dioxide. Science 213: 957–966

Hansen JD, Lacis A, Rind D, Russell G, Stone P, Fung I, Ruedy R, Lerner J (1984) In: Hansen JE, Takahashi T (eds) Climate processes and climate sensitivity. American Geophysical Union, Washington DC, pp 130–163

Harrison EF, Minnis P, Barkstrom BR, Ramanathan V, Cess RD, Gibson GG (1990) Seasonal variation of cloud radiative forcing derived from the Earth Radiation Budget Experiment. J Geophys Res 95: 18 687–18 703

Ingram WJ, Wilson CA, Mitchell JFB (1989) Modelling climate change: an assessment of sea ice and surface albedo feedbacks. J Geophys Res 94: 8609–8622

IPCC (1990) Climate Change The IPCC scientific assessment. Houghton JT, Jenkins GJ, Ephraums JJ (eds) Cambridge University Press, 365 pp

IPCC (1996) Climate change 1995 The science of climate change. Houghton JT, Meira Filho LG, Callander BA, Harris N, Kattenberg A, Maskell K (eds) Cambridge University Press, 572 pp

Kiehl JT, Briegleb BP (1993) The relative role of sulphate aerosols and greenhouse gases in climate forcing. Science 260: 311–314

Le Treut H, Li ZX, Forichon M (1994) Sensitivity study of the LMD GCM to greenhouse forcing associated with two different cloud water parametrizations. J Clim 7: 1827–1841

Lee WH, Iacobellis AF, Somerville RCJ (1997) Cloud radiation forcings and feedbacks: general circulation model tests and observational validation. J Clim 10: 2479–2496

Lemus L, Rikus L, Fraser J, Sun Z (1997) Cloud optical properties for UV-SW-LW radiation: three forecast experiments. Proc WMO Workshop on Measurements of Cloud Properties for Forecasts of Weather and Climate, Mexico City, 23–27 June 1997, Baumgardener D, Raga G (eds) pp 312–320

Li Z-X, Le Treut H (1992) Cloud-radiation feedbacks in a general circulation model and their dependence on cloud modelling assumptions. Clim Dyn 7: 133–139

Louis J-F (1983) Parametrization of sub-grid scale processes ECMWF Seminar, 13–17 September, 1982 and Workshop, 20–24 September, 1982, ECMWF, Reading, England: 83–97

Manabe S, Holloway JL (1975) The seasonal variation of the hydrological cycle as simulated by a global model of the atmosphere. J Geophys Res 80: 1617–1649

Martin GM, Johnson DW, Spice A (1994): The measurement and parametrization of effective radius of droplets in warm stratocumulus clouds. J Atmos Sci 51: 1823–1842

McAvaney BJ, Colman RA (1996) Water vapor and cloud feedbacks in the BMRC GCM, In: Le Treut H (ed) Climate Sensitivity to Radiative Perturbations Physical Mechanisms and their Validation. NATO ASI vol I 34, Springer, Berlin, Heidelberg New York, pp 171–190

McAvaney BJ, Hess GD (1996) The revised surface fluxes parametrization in BMRC: formulation. BMRC Research Report 56: Bur Meteorol Australia

Miller MJ, Beljaars ACM, Palmer TN (1992) The sensitivity of the ECMWF model to the parametrization of evaporation from the tropical ocean. J Clim 5: 418–434

Mitchell JFB, Ingram WJ (1992) Carbon dioxide and climate: Mechanisms of changes in cloud. J Clim 5: 5–21

Mitchell JFB, Senior CA, Ingram WF (1989) CO_2 and climate a missing feedback? Nature 341: 132–134

Palmer TN, Shutts GJ, Swinbank R (1986) Alleviation of a systematic bias in general circulation and numerical weather prediction models through an orographic gravity wave drag parametrization. Q J R Meteorol Soc 112: 1001–1039

Platt CMR (1994) Parametrization of cloud-radiation interactions from observations. Parametrization of physical process, Papers presented at the fifth BMRC Modelling Workshop, November 1993, Jasper JD, Meighen PJ (eds) BMRC, GPO Box 1289K, Melbourne, 3001, Australia, 153–158

Platt CMR (1989) The role of cloud microphysics in high-cloud feedback effects on climate change. Nature 341: 428–429

Platt CMR, Stephens GL (1980) The interpretation of remotely sensed high cloud emittances. J Amos. Sci 37: 2314–2322

Pollack JB, Rind D, Lacis A, Hansen JE, Sato M, Ruedy R (1993) GCM simulations of volcanic aerosol forcing. Part I climate changes induced by steady-state perturbations. J Clim 6: 1719–1742

Ramanathan V, Barkstrom BR, Harrison EF (1989) Climate and the Earth's radiation budget. Phys Today 42: (5) 22–32

Randel D, Von der Haar TH, Ringerud MA, Stephens GL, Greenwald TJ, Combs CL (1996) A new global water vapor dataset. Bull Am Meteorol Soc 77: 1233–1246

Roeckner E, Schlese U, Biercamp J, Loewe P (1987) Cloud optical depth feedbacks and climate modelling. Nature 329: 138–140

Rossow WB, Schiffer RA (1991) ISCCP cloud data products. Bull Am Meteorol Soc 72: 2–20

Rotstayn LD (1997) A physically based scheme for the treatment of stratiform clouds and precipitation in large-scale models. 1: description and evaluation of the microphysical processes. Q J R Meteorol Soc 123: 1227–1282

Rotstayn LD (1999) Climate sensitivity of the CSIRO GCM: effect of cloud modeling assumptions. J Clim 12: 334–356

Schlesinger ME (1988) Quantitative analysis of feedbacks in climate model simulations of CO_2 induced warming. In: Schlesinger ME (ed) Physically based modelling and simulation of climate and climate change, NATO ASI Series C, vol 243 Kluwer Academic Publishers, Dordrecht

Schlesinger ME, Roeckner E (1988) Negative or positive cloud optical depth feedback? Nature 335: 303–304

Schwarzkopf MD, Fels SB (1991) The simplified exchange method revisited: an accurate, rapid method for computation of infrared cooling rates and fluxes. J Geophys Res 96: 9075–9096

Senior CA, Mitchell JFB (1993) Carbon dioxide and climate: the impact of cloud paramatrization. J Clim 6: 393–418

Slingo A (1989) A GCM parametrization for the shortwave radiative properties of water clouds. J Atmos Sci 46: 1419–1427

Smith RNB (1990) A scheme for predicting layer clouds and their water content in a general circulation model. Q J R Meteorol Soc 116: 435–460

Somerville RCJ, Remer LA (1984) Cloud optical thickness feedbacks in the CO_2 climate problem. J Geophys Res 89: 9668–9672

Stephens GL, Greenwald TJ (1991) The Earth's radiation budget and its relation to atmospheric hydrology, I, Observations of the, clear-sky greenhouse effect. J Geophys Res 96: 15 311–15 324

Stowe LL, Yeh HYM, Eck TF, Wellemeyer CG, Kyle HL and the Nimbus-7 Cloud Data processing Team (1989) Nimbus-7 cloud climatology, Part II. J Clim 2: 671–709

Sun Z, Shine KP (1994) Studies of the radiative properties of ice and mixed-phase clouds. Q J R Meteorol Soc 120: 111–137

Taylor KE, Ghan SJ (1992) An analysis of cloud liquid water feedback and global climate sensitivity in a general circulation model. J Clim 5: 907–919

Tiedtke M (1988) Parametrization of cumulus convection in large-scale models. In: Schlesinger M (ed) Physically based modelling and simulation of climate and climatic change – Part I. Kluwer Academic; Dordrecht, pp 375–431

Tiedtke M (1989) A comprehensive mass flux scheme for cumulus parametrization in large-scale models. Mon Weather Rev 117: 1779–1800

Tselioudis G, Del Genio AD, Kovari W, Yao M-S (1998) Temperature dependence of low cloud optical thickness in the GISS GCM: contributing mechanisms and climate implications. J Clim 11: 3268–3281

Warren SG, Hahn CJ, London J, Chervin RM, Jenne RL (1986) Global distribution of total cloud cover and cloud type amounts over land, NCAR Technical Note TN-273-STR, Boulder CO, 224 pp

Warren SG, Hahn CJ, London J, Chervin RM, Jenne RL (1988) Global distribution of total cloud cover and cloud type amounts over the ocean, NCAR Technical Note TN317 + STR, Boulder CO, 212 pp

Washington WM, Meehl GA (1986) GCM CO_2 sensitivity experiments: snow-sea-ice parametrizations and globally averaged surface air temperature. Clim Change 8: 231–241

Watterson IG, Dix MR, Colman RA (1999) A comparison of present and doubled CO_2, climates and feedbacks simulated by three GCMs. J Geophys Res 104: 1943–1956

Weng F, Grody NC (1994) Retrieval of cloud liquid water using the Special Sensor Microwave Imager (SSM/I). J Geophys Res 99: 25 535–25 551

Wetherald RT, Manabe S (1986) An investigation of cloud cover change in response to thermal forcing. Clim Change 8: 5–24

Wetherald RT, Manabe S (1988) Cloud feedback processes in a GCM. J Atmos Sci 45: 1397–1415

Yao M-S, Del Genio AD (1999) Effects of cloud parametrization on the simulation of climate changes in the GISS GCM. J Clim 12: 761–779

Zhang MH, Cess RD, Hack JJ, Kiehl JT (1994) Diagnostic study of climate feedback processes in atmospheric general circulation models. J Geophys Res 99: 5525–5537